PHILOSOPHICAL MAGAZINE, 21 NOVEMBER 2004
VOL. 84, NO. 33, 3517–3546

Taylor & Francis
Taylor & Francis Group

Deformation banding under arbitrary monotonic loading in cubic metals

S. MAHESH and C. N. TOMÉ*

MST-8, Los Alamos National Laboratory, Los Alamos, NM 87545, USA

[*Received 2 March 2004 and accepted 21 April 2004*]

ABSTRACT

We present a Taylor-based theory of deformation of an aggregate of rigid-plastic crystals that allows for heterogeneity of grain deformation, and use it to model macroscopic subdivision of grains into mutually misoriented volumes, a process termed deformation banding. Each grain is assumed to accommodate the macroscopically imposed deformation such that the power of its plastic deformation is minimized. This minimization may involve the formation of deformation bands. The theory is applied to tension, compression and rolling of fcc aluminium and bcc α-iron polycrystals, and used to predict the macroscopic mechanical response, the polycrystal texture, the orientation of deformation bands, and the misorientations across them. These predictions are compared with experimental observations available in the literature, and good qualitative agreement is found.

§ 1. INTRODUCTION

Most polycrystal plasticity models assume that grains deform homogeneously within the aggregate. While this assumption is reasonably successful in predicting polycrystal behaviour during plastic deformation, and in capturing the major texture components, it often results in quantitative and qualitative differences between the measured and calculated texture and flow response. For example, the predicted textures are systematically sharper than those measured, and certain experimentally observed texture components are not predicted (Lee and Duggan 1993). As a consequence, some researchers have started, in recent years, to incorporate more detailed descriptions of the dislocation structure and inhomogeneous grain deformation in their models (Lee and Duggan 1993, Peeters *et al*. 2001, Mahesh *et al*. 2005).

In this paper we propose a model for describing grain banding and evolution of misorientation, based on an energy minimization criterion. We apply this model to the simulation of tensile, compressive and plane strain deformation of polycrystalline aggregates of cubic structure. It is important to emphasize that our criterion is applicable to the 'mesoscopic' length scale, where the intergranular interactions control the deformation, and not to the 'microscopic' scale, where energy minimization taking place through dislocation rearrangement is driven by local stresses. The following discussion clarifies this point.

During plastic deformation, grains of cubic metals with medium-to-high stacking fault energy form relatively misoriented domains, each of which may undergo plastic

*Author for correspondence. Email: tome@lanl.gov.

Philosophical Magazine ISSN 1478–6435 print/ISSN 1478–6443 online
http://www.tandf.co.uk/journals
DOI: 10.1080/14786430412331297500

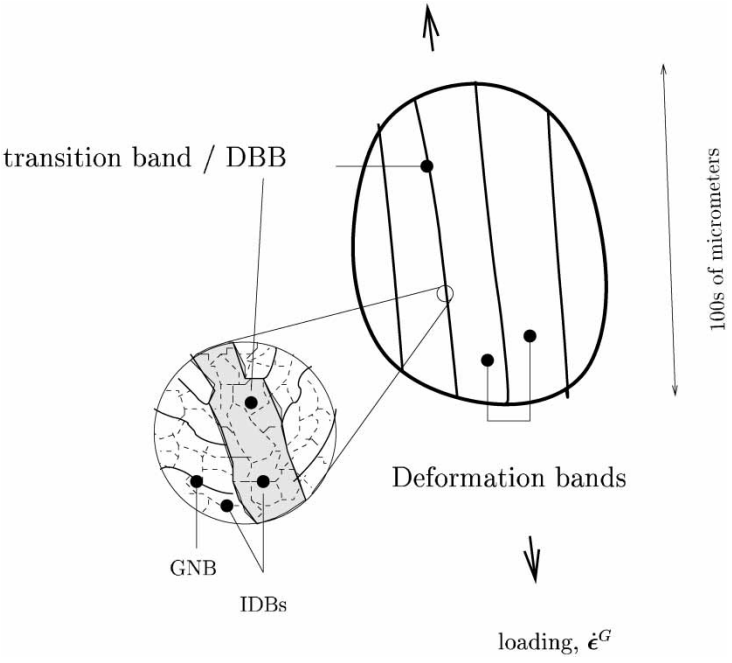

Figure 1. Schematic of the dislocation substructure within a moderate- or large-sized grain, showing deformation bands (see figure 8 in Kulkarni *et al.* (1998) for a micrograph), and an enlarged view of the substructure near a deformation band boundary, drawn here as a transition band (also see figure 19 in Liu and Hansen (1998)). The substructure shown is characteristic of small-to-moderate deformations ($\lesssim 30\%$ von Mises strain for Al) with a cell and cell-block structure. IDBs enclosing cells are shown as dashed lines, and GNBs enclosing cell blocks as solid lines. The transition band is shown shaded in the enlarged view, and is subdivided largely by dislocation cells. On the other hand, the deformation bands are shown divided by both cells and cell blocks in keeping with the observations of Liu and Hansen (1998).

deformation different from the grain average (Bay *et al.* 1992, Hughes and Hansen 1993). The subdivision into domains is effected over a wide range of length scales (see figure 1). The smallest subdivision is by incidental dislocation boundaries (IDBs) that arise from statistical trapping of glide dislocations. IDBs form dislocation cells and engender small lattice misorientations across themselves about a uniformly distributed random axis. On a larger length scale, geometrically necessary boundaries (GNBs) subdivide a grain by enclosing a group of cells, sometimes called a cell-block. GNBs form so as to accommodate deformation gradients in the flow field (Argon 2002, Dawson *et al.* 2002) and, therefore, they tend to be preferentially oriented. The average misorientation across GNBs is larger than that across IDBs, and scales as a power law with grain strain (Hughes *et al.* 1997). Thus, commonly, IDBs separate lattice regions that have the same active slip systems deforming with different shear amplitudes, while the domains separated by GNBs have differing slip system activities (Bay *et al.* 1992).

GNB structure displays considerable variety at any given strain, and also shows qualitative structural transitions with increasing strain. For reasons to be given below, a GNB structure of particular interest to this work is the deformation band (DB), visible even in optical micrographs of single crystals or large-grained

polycrystals (diameter $\gtrsim 100\,\mu m$, see figure 1). DBs are the largest GNBs in such crystals, and enclose volumes only one or two orders of magnitude smaller than that of the grain itself. They have been described as 'slab-like' or 'lath'-shaped alternating regions, that extend across the grain (i.e. terminate at grain boundaries (Kulkarni and Kuhlmann-Wilsdorf 1998)). DBs are precursors of independent grains (Duggan and Lee 1996). The dislocation structure enclosing a DB may either be sharp or diffuse (Duggan and Lee 1993), and will be referred to as a deformation band boundary (DBB). If a DBB is diffuse and has width comparable to the DB itself, it has been called a transition band (Liu and Hansen 1998, Hansen and Jensen 1999). A smooth transition between the lattice orientations of adjacent DBs is accomplished over the thickness of a DBB.

The number of DBs in a grain has been found to be unvarying with applied strain (Lee *et al.* 1993, Liu and Hansen 1998). It is important that DBBs not be confused with the elongated 'lamellar boundaries' studied by Hughes and Hansen (1993): firstly, DBBs separate grain volumes much larger than those separated by lamellar boundaries, and, secondly, grain subdivision into DBs takes place even at small strains (15% cold rolling of Al; see Liu and Hansen (1988)), whereas lamellar boundaries are characteristic of high-strain substructures.

The definition of a DB varies in the literature. Barrett (1939) and Barrett and Levenson (1940) studied the largest dislocation structures through optical microscopy in iron and aluminium, respectively, and coined the term *deformation bands* for the misoriented lattices. They also found 'fine structure' within the deformation bands, which have since been revealed as smaller dislocation structures using electron microscopy (Hughes and Hansen 1993). Although Barrett and Levenson applied the term 'deformation bands' to these smaller dislocation structures as well, later authors have primarily used it to denote macroscopic subdivision of grains. Our definition keeps with this later trend. We will call the largest dislocation structures deformation band boundaries (DBBs), and the volumes they separate deformation bands (DBs) if (i) they deform differently than the grain on average, and (ii) their minimum dimension is much larger than the mean free path of dislocations. Hansen and Jensen (1999) and Kuhlmann-Wilsdorf (1999a) have recently surveyed the phenomenon of deformation banding.

An energy criterion for deformation banding was given by Chin and Wonsiewicz (1969). Loosely, it states that if the deformation energy or power can be sufficiently lowered by inhomogeneous grain deformation below that of homogeneous deformation, then the former will be favoured. Different authors have proposed different energies of deformation associated with this criterion. Lee and Duggan (1993), Lee *et al.* (1993), Ortiz and Repetto (1999), and Ortiz *et al.* (2000) have defined it as the *total* plastic work of deformation, and deformation banding in their models is a result of *latent hardening*. Kuhlmann–Wilsdorf's (1999a) model of deformation banding is similar to that of Chin and Wonsiewicz, except that, instead of the plastic power, she considers the stored elastic strain energy as the quantity to be minimized.

Experimentally, much recent work has focused on the study of the grain substructure that forms during plastic deformation over a range of imposed deformation conditions in both single and polycrystals (Huang and Hansen 1997, Winther *et al.* 1997, 2000, Christoffersen and Leffers 1998, Huang 1998, Wert 2002, Wert and Huang 2003). These works have focused on the length scale of the smallest GNB, i.e. at length scales comparable to the mean free path of dislocations ($< 5\,\mu m$ in aluminium deformed a few percent), and attempt to find patterns in the experi-

mentally observed microstructure. However, the phenomenological rules for the character of the microstructures that have emerged from these efforts are only applicable to certain specific deformation conditions on specific materials. No satisfactory general pattern of GNB position and orientation over arbitrary loading on arbitrarily oriented grains has been proposed yet, nor is there an encompassing theory to explain the variations.

The energy criterion mentioned above does not include dislocation kinetics, and cannot be expected to reliably predict GNB character at length scales comparable to the mean free path of individual dislocations. To see why, we recall Winther's (2003) observation that the microstructure at any length scale is influenced both by a 'crystallographic preference' and a 'macroscopic preference'. The crystallographic preference derives from the tendency of the dislocations available from slip activity to form local, low-energy dislocation structures (Kuhlmann–Wilsdorf 1999b), while the macroscopically preferred orientation is governed by macroscopic effects such as loading direction and grain orientation. DBBs, being much larger than the dislocation mean free path, can be expected to be least influenced by the crystallographic preference, and form in a manner dominated by the macroscopic preference. As a consequence, the formation of 'macroscopic' DBBs can be studied separately from the 'microscopic' GNBs. DBs are also attractive from the perspective of polycrystal plasticity modelling because, being the largest dislocation structures, they are expected to have a greater influence on polycrystal texture and grain fragmentation than smaller misoriented volumes.

In this work, we restrict ourselves to modelling deformation banding, dominated by the macroscopic preference, and do not venture to model the competition between the crystallographic and macroscopic preferences to predict the orientations of GNBs smaller than DBs. In the following, we develop a theory of inhomogeneous grain deformation following the Chin–Wonsiewicz criterion, for rigid-plastic grains deforming according to the macroscopically imposed velocity gradient (Taylor polycrystal). In section 2 we collect relevant facts concerning deformation banding from previous works. Section 3 details the theory, and section 4 presents its predictions. Section 5 discusses these results and compares them with previous theories.

§ 2. Previous work on deformation banding

Experimental work on DBs has been done both on polycrystals and on single crystals. Barrett (1939) and Barrett and Levenson (1940) first recognized the inhomogeneity of grain deformation in mild steel and aluminium, respectively, and ruled out twinning as its cause. More recently, Lee, Duggan and co-workers have extensively studied deformation banding during cold rolling of fcc copper polycrystals (Lee and Duggan 1993, Lee *et al*. 1993, 1995) and Duggan and co-workers have studied bcc steel (Tse *et al*. 2000, Liu and Duggan 2001). They observe a three-dimensional arrangement of lath-shaped DB, each spanning the length of the grain in the longitudinal section.

An experimental deformation banding study during uniaxial compression of aluminium was carried out by Kulkarni and Kuhlmann-Wilsdorf (1998). They observe primary, secondary and even tertiary DB, nested within each other, and a grain size dependence of the number of bands.

Akef and Driver (1991), Maurice and Driver (1993), and Basson and Driver (2000) have conducted detailed experimental studies of the deformation banding of cube oriented fcc *single crystals* subjected to channel-die compression. They

find that, depending on the metal, deformation bands form after a certain amount of strain, with the DBBs perpendicular to the transverse direction (TD). Using the Bishop–Hill crystal plasticity theory, they explain the rotations of the deformation bands (after their formation) as due to spatial separation of the slip system activity needed to accommodate the imposed deformation. An important observation of these authors is that, once bands form, they rapidly rotate about the TD relative to each other. In the nominally identical plane strain loading under rolling, Liu and Hansen (1998) and Liu *et al.* (2000) have studied the development of macroscopic misorientations in cube oriented aluminium single crystals. Although they too find that bands rotate about the TD, their DBBs form perpendicular to the normal direction (ND). They ascribed the observed misorientation development to location-dependent shear stresses (Lee and Duggan 1991) imposed during rolling deformation.

On the theoretical side, an energy-based criterion for the formation of deformation bands was proposed by Chin and Wonsiewicz (1969) to explain the phenomenon observed experimentally (Ahlborn 1966a,b) in axisymmetric wire drawing. Their framework has been retained by all succeeding authors and indeed underlies the present work. Expressed in terms of deformation rates instead of infinitesimal deformation increments, it states that a grain will band during plastic deformation if the power required to accomplish a certain shape change by homogeneous deformation, $\dot{W}_{\mathrm{H}} = \sum_s \tau_s \dot{\gamma}_s$, exceeds that by banded deformation. Here, τ_s and $\dot{\gamma}_s$ denote the critical resolved shear stress and the slip strain rate on slip system s, respectively. The latter power consists of (1) $\dot{W}_{\mathrm{i}}$, the power of slip within the bands, (2) $\dot{W}_{\mathrm{b}}$, the power associated with the formation of a boundary between bands, and (3) $\dot{W}_{\mathrm{c}}$, the power to correct the difference in shape arising from banding and homogeneous deformation. Thus, the Chin–Wonsiewicz condition for grain banding is that

$$\dot{W}_{\mathrm{B}} = \dot{W}_{\mathrm{i}} + \dot{W}_{\mathrm{b}} + \dot{W}_{\mathrm{c}} < \dot{W}_{\mathrm{H}}. \tag{1}$$

Chin and Wonsiewicz did not compute $\dot{W}_{\mathrm{b}}$ and $\dot{W}_{\mathrm{c}}$. However, they show that Ahlborn's experimental observations satisfy $\dot{W}_{\mathrm{i}} < \dot{W}_{\mathrm{H}}$, which is necessary if equation (1) is to be satisfied.

In their model of deformation banding, Lie and Duggan (1993) and Lee *et al.* (1993) minimize the internal *work* of plastic deformation, over finite deformation steps. Their model grains experience latent hardening on all non-primary slip planes. If $\Delta\gamma_s$ is the deformation increment over a finite deformation step on slip system s, τ_s the critical resolved shear stress (CRSS) at the beginning of that step, and $h_{ss'}$ the latent hardening coefficient between slip systems s and s', then the average CRSS over that step is $\tau_s + (1/2)\sum_{s'} h_{ss'}\Delta\gamma_{s'}$. Thus, the work of incremental plastic deformation is

$$\Delta W = \sum_s \tau_s \Delta\gamma_s + (1/2)\sum_s \sum_{s'} h_{ss'}\Delta\gamma_s\Delta\gamma_{s'}. \tag{2}$$

In their model, latent hardening drives deformation banding, since slip on multiple planes may be avoided in different bands while still accommodating the imposed grain deformation on average over all bands. This way, the otherwise large work of deformation due to latent hardening can be lowered by suppressing latent hardening in individual bands. The minimization in Lee and Duggan's model is carried out subject to the constraint that DBBs are oriented perpendicular to the TD. They fix the extensional strains in both DBs to be the same as that of the grain, but relax

the shear strain components in each DB in the planes perpendicular to the TD and rolling direction (RD) using relaxed constraints (RCs). They then require that the shear strain components in the plane perpendicular to ND cancel out between the two sub-grains. They also compute the accommodation energy W_b in the Chin–Wonsiewicz condition using Read and Shockley's (1950) formula for the surface energy associated with a low-angle grain boundary and W_c as the elastic energy stored due to forcing displacement compatibility at the ends of flat deformation bands aligned with the rolling direction. Using this theory, they find that increasing numbers of grains band with continued deformation. They also find that the formation of bands is sensitive to the grain orientation relative to loading.

The theory of Ortiz and Repetto (1999) and Ortiz *et al.* (2000) extends that of Lee and Duggan by removing many of the restrictive assumptions. It allows for the formation of nested deformation bands, arbitrary DBB orientation and arbitrary monotonic loading paths. The accommodation terms are treated quite differently than in the theory of Lee *et al.* In the theory of Ortiz *et al.* also, latent hardening drives microstructuring; its absence will result in homogeneous deformation.

The minimization of ΔW in equation (2) inherently involves 'looking ahead' in the deformation by a finite $\Delta\gamma_s$ to determine whether it would be energetically beneficial to band or not at a certain instant during the deformation. It is essential that $\Delta\gamma_s$ be non-infinitesimal in order that the second term in equation (2) influence ΔW. For, in the limit $\Delta\gamma_s \downarrow 0$, the second term scales as a quadratic in $\Delta\gamma_s$ and diminishes more rapidly than the linearly diminishing first term in equation (2). In this limit, the above theories predict no deformation banding. Thus, in addition to the physical grain's dislocation substructure at a certain instant (as indirectly quantified by the CRSS of its slip systems), its deformation banding criterion according to the above theories seemingly involves foresight of its future deformation.

It should be emphasized that the validity of the above theories or of their energy criteria is not being questioned here. Latent hardening in these theories is used simply as an abstract *model* of the experimental fact that grains prefer to use a smaller number of slip systems, and is not to be viewed as advance knowledge supplied to the grain on its forthcoming deformation. Nevertheless, in our view, a theory that supplies a *physical mechanism* for lowering the number of active slip systems involving only the present state of the grain, without recourse to its future deformation, would be more physically grounded. Such a mechanism (which naturally cannot hinge on latent hardening, but which does not exclude latent hardening either) and theory of deformation banding will be presented next. The key idea is that macroscopic DBs are assumed to be 'seeded' by misorientation across IDBs, which may develop into substantially misoriented GNBs if doing so is energetically favourable. It will turn out that the number of active slip systems in each band will be reduced from the number needed in homogeneous deformation, just as in the theory of Lee and Duggan. We also note here that the present deformation banding criterion does not hinge on (but does not forbid either) the rate sensitivity of the grain constitutive law.

§ 3. The deformation banding theory

3.1. *Assumptions*

We collect some definitions and assumptions regarding the deformation of individual grains and their interaction with each other in a polycrystal here.

Consider a grain, each of whose S slip system orientations have unit normal $\mathbf{n}^s$ and Burgers vector $\mathbf{b}^s$. The Schmid tensor ($\mathbf{m}^s$, $s = 1, \ldots, S$) is given by (Kocks *et al.* 1998)

$$\mathbf{m}^s = (\mathbf{n}^s \otimes \mathbf{b}^s + \mathbf{b}^s \otimes \mathbf{n}^s)/2. \tag{3}$$

If $\dot{\gamma}^s$ denotes the slip rate on slip system s, $s = 1, 2, \ldots, S$, then the velocity gradient is

$$\mathbf{L} = \sum_{s=1}^{S} \dot{\gamma}^s \mathbf{b}^s \otimes \mathbf{n}^s, \tag{4}$$

and the strain rate tensor in the grain is given by

$$\dot{\boldsymbol{\varepsilon}} = \sum_{s=1}^{S} \dot{\gamma}^s \mathbf{m}^s = \operatorname{sym} \mathbf{L}. \tag{5}$$

The deformation gradient $\mathbf{F}$ of the grain has a rate of change (Gurtin 1981) given by

$$\dot{\mathbf{F}} = \mathbf{L}\mathbf{F}. \tag{6}$$

In an incremental implementation of crystal plasticity, as done in the present work, equation (6) is used to generate a linear extrapolation of the deformation gradient of the grain. Let $\mathbf{L}^k$ and $\mathbf{F}^k$ be the velocity and deformation gradients at time step k, and let t_k be the time of the kth increment (Kocks *et al.* 1998). Then,

$$\mathbf{F}^{k+1} = \mathbf{F}^k + (t_{k+1} - t_k)\mathbf{L}^k\mathbf{F}^k \tag{7}$$

represents a good approximation of $\mathbf{F}^{k+1}$ for small $t_{k+1} - t_k$.

Throughout, we ignore elastic deformations; the grain constitutive response is assumed to be rigid-plastic following the viscoplastic constitutive law proposed by Hutchinson (1976), Asaro and Needleman (1985) and Canova *et al.* (1988):

$$\dot{\gamma}^s = \left| \frac{\boldsymbol{\sigma} : \mathbf{m}^s}{\tau^s} \right|^n \operatorname{sign}(\boldsymbol{\sigma} : \mathbf{m}^s), \qquad s = 1, 2, \ldots, S. \tag{8}$$

$\boldsymbol{\sigma}$ is the *deviatoric* stress experienced by the grain, $\tau^s > 0$ is the critical resolved shear stress on slip system s, and n the reciprocal rate sensitivity. As $n \uparrow \infty$, the material becomes rate-insensitive. We will assume $n > 2$. Using equations (5) and (8), we get

$$\dot{\boldsymbol{\varepsilon}} = \sum_{s=1}^{S} \mathbf{m}^s \left| \frac{\boldsymbol{\sigma} : \mathbf{m}^s}{\tau^s} \right|^n \operatorname{sign}(\boldsymbol{\sigma} : \mathbf{m}^s). \tag{9}$$

Since the symmetric $\dot{\boldsymbol{\varepsilon}}$ denotes the plastic strain rate, it is volume preserving so that $\operatorname{Tr} \dot{\boldsymbol{\varepsilon}} = 0$. Thus, $\dot{\boldsymbol{\varepsilon}}$ can be fully specified using five independent coordinates, and we will use the Leibfried and Breuer representation (Kocks *et al.* 1998, chap. 7) of $\dot{\boldsymbol{\varepsilon}}$ as a 5-tuple. It is important to note that this representation is basis-dependent, i.e. it does not transform tensorially. In this scheme, $[\dot{\boldsymbol{\varepsilon}}] = \dot{\epsilon}_{ij}$ has the representation

$$\{\dot{\epsilon}_\lambda\} = \left\{ \frac{\dot{\epsilon}_{22} - \dot{\epsilon}_{11}}{\sqrt{2}}, \frac{2\dot{\epsilon}_{33} - \dot{\epsilon}_{22} - \dot{\epsilon}_{11}}{\sqrt{6}}, \sqrt{2}\dot{\epsilon}_{23}, \sqrt{2}\dot{\epsilon}_{13}, \sqrt{2}\dot{\epsilon}_{12} \right\}, \tag{10}$$

and $[\boldsymbol{\sigma}] = \sigma_{ij}$ the representation

$$\{\sigma_\lambda\} = \left\{ \frac{\sigma_{22} - \sigma_{11}}{\sqrt{2}}, \frac{2\sigma_{33} - \sigma_{22} - \sigma_{11}}{\sqrt{6}}, \sqrt{2}\sigma_{23}, \sqrt{2}\sigma_{13}, \sqrt{2}\sigma_{12} \right\}, \tag{11}$$

where $\lambda = 1, 2, \ldots, 5$. The summation convention over repeated indices will be used, except when the index identifies a slip system.

§ 3.2. The banding condition

Except for the work of Lee, Duggan and co-workers, the Chin–Wonsiewicz condition has only been used to verify that equation (1) holds in particular experimentally observed banding grains. Lee and Duggan (1993) were the first to calculate the band deformations as those that minimize $\dot{W}_{\mathrm{B}}$, subject to the constraint that the imposed grain deformation is accommodated on average by the bands. Lee *et al.* (1995) later observed that $\min \dot{W}_{\mathrm{i}} < \dot{W}_{\mathrm{H}}$ very likely implies $\min \dot{W}_{\mathrm{B}} < \dot{W}_{\mathrm{H}}$.

We presently give a formula for the terms in $\dot{W}_{\mathrm{B}}$, and describe a simplified approximate methodology to compute $\min \dot{W}_{\mathrm{B}}$, by sequentially minimizing $\dot{W}_{\mathrm{i}}$, and then $\dot{W}_{\mathrm{b}} + \dot{W}_{\mathrm{c}}$. The negligibility of $\dot{W}_{\mathrm{b}} + \dot{W}_{\mathrm{c}}$ compared to $\dot{W}_{\mathrm{i}}$, which justifies this approximation, was observed by Lee *et al.* (1995). We will show *a posteriori* that, in the present calculation also, sequential minimization of $\dot{W}_{\mathrm{B}}$ should result in no significant errors.

3.2.1. *Plastic power* ($\dot{W}_i$)

Consider a grain on which strain rate $\dot{\boldsymbol{\varepsilon}}^{\mathrm{G}}$ is imposed. The corresponding stress $\boldsymbol{\sigma}^{\mathrm{G}}$ is given by the viscoplastic constitutive law equation (9). The plastic power of the grain under homogeneous deformation $\dot{W}_{\mathrm{H}}$ is then

$$\dot{W}_{\mathrm{H}}(\dot{\boldsymbol{\varepsilon}}^{\mathrm{G}}) = \boldsymbol{\sigma}^{\mathrm{G}} : \dot{\boldsymbol{\varepsilon}}^{\mathrm{G}} = \sum_{s=1}^{S} \tau_s \left| \frac{\boldsymbol{\sigma}^{\mathrm{G}} : \mathbf{m}^s}{\tau^s} \right|^{n+1} = \sum_{s=1}^{S} \tau^s |\dot{\gamma}^s|^{1+1/n}. \tag{12}$$

To simplify the consideration of inhomogeneous deformation under an imposed $\dot{\boldsymbol{\varepsilon}}^{\mathrm{G}}$, we model the grain as a pair of bands, each of which has the same lattice orientation as the original (homogeneously deforming) grain. Let the pair of bands have volume fractions w and $1 - w$ relative to the grain volume, $0 \leq w \leq 1$. If $\dot{\boldsymbol{\varepsilon}}^{(1)}$ and $\dot{\boldsymbol{\varepsilon}}^{(2)}$ are the strain rates of each of the bands, then the full constraints condition (Hill 1967) requires that

$$w\dot{\boldsymbol{\varepsilon}}^{(1)} + (1 - w)\dot{\boldsymbol{\varepsilon}}^{(2)} = \dot{\boldsymbol{\varepsilon}}^{\mathrm{G}}. \tag{13}$$

If the stresses corresponding to $\dot{\boldsymbol{\varepsilon}}^{(1)}$ and $\dot{\boldsymbol{\varepsilon}}^{(2)}$ computed according to equation (9) are $\boldsymbol{\sigma}^{(1)}$ and $\boldsymbol{\sigma}^{(2)}$, respectively, then the plastic power of banded deformation is

$$\dot{W}_{\mathrm{i}}(w, \dot{\boldsymbol{\varepsilon}}^{(1)}, \dot{\boldsymbol{\varepsilon}}^{(2)}) = w\boldsymbol{\sigma}^{(1)} : \dot{\boldsymbol{\varepsilon}}^{(1)} + (1 - w)\boldsymbol{\sigma}^{(2)} : \dot{\boldsymbol{\varepsilon}}^{(2)}. \tag{14}$$

In applying equation (9) to compute $\boldsymbol{\sigma}^{(1)}$ and $\boldsymbol{\sigma}^{(2)}$ given $\dot{\boldsymbol{\varepsilon}}^{(1)}$ and $\dot{\boldsymbol{\varepsilon}}^{(2)}$, respectively, we assume that τ^s and $\mathbf{m}^s$, $s = 1, \ldots, S$, in both bands have the same value as that in the homogeneous grain. It should be noted that the domain undergoing deformation with strain rate $\dot{\boldsymbol{\varepsilon}}^{(1)}$ or $\dot{\boldsymbol{\varepsilon}}^{(2)}$ need not be contiguous for equation (14) to hold. In fact, we will later regard the grain subdivided as shown in figure 2, consisting of bands alternately deforming with strain rate $\dot{\boldsymbol{\varepsilon}}^{(1)}$ and $\dot{\boldsymbol{\varepsilon}}^{(2)}$. It is only important for the validity of equation (14) that the volume fraction of all bands deforming with strain rate $\dot{\boldsymbol{\varepsilon}}^{(1)}$ add up to w, and those deforming with $\dot{\boldsymbol{\varepsilon}}^{(2)}$ add up to $1 - w$.

Now, $\dot{W}_{\mathrm{H}}(\dot{\boldsymbol{\varepsilon}}^{\mathrm{G}})$ in equation (12) is convex in $\dot{\boldsymbol{\varepsilon}}^{\mathrm{G}}$ (Ortiz and Repetto 1999), i.e. given any strain rates $\dot{\boldsymbol{\varepsilon}}^{(1)}$ and $\dot{\boldsymbol{\varepsilon}}^{(2)}$ satisfying equation (13),

$$\begin{aligned} \dot{W}_{\mathrm{i}}(w, \dot{\boldsymbol{\varepsilon}}^{(1)}, \dot{\boldsymbol{\varepsilon}}^{(2)}) &= w\dot{W}_{\mathrm{H}}(\dot{\boldsymbol{\varepsilon}}^{(1)}) + (1 - w)\dot{W}_{\mathrm{H}}(\dot{\boldsymbol{\varepsilon}}^{(2)}) \\ &\geq \dot{W}_{\mathrm{H}}[w\dot{\boldsymbol{\varepsilon}}^{(1)} + (1 - w)\dot{\boldsymbol{\varepsilon}}^{(2)}] = \dot{W}_{\mathrm{H}}(\dot{\boldsymbol{\varepsilon}}^{\mathrm{G}}), \end{aligned} \tag{15}$$

which rules out satisfaction of the Chin–Wonsiewicz condition, equation (1).

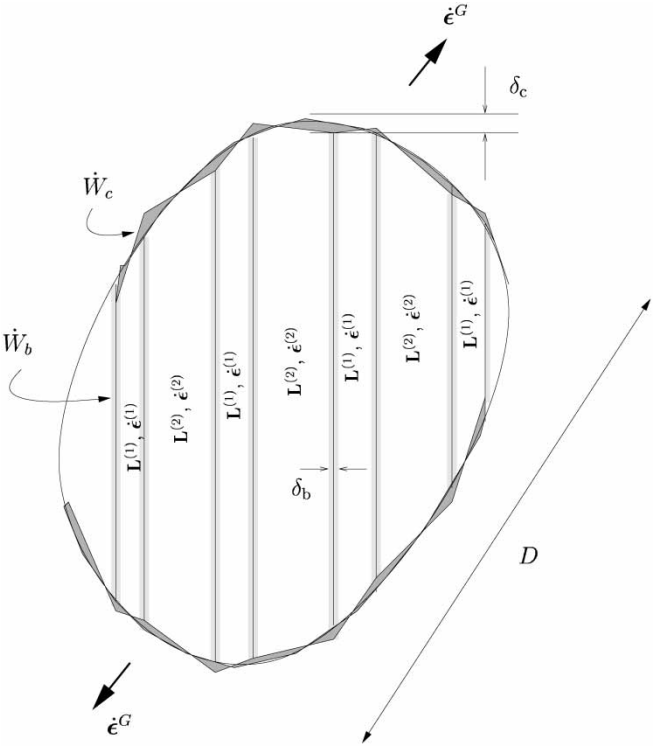

Figure 2. An accommodation band (shown shaded) is typically needed for strain compatibility across grain boundaries and between bands in banded grains, wherein power $\dot{W}_c$ and $\dot{W}_b$, respectively, is stored. As shown, the grain has $N = 8$ DBB and $N + 1 = 9$ DBs. The DBs may have differing volume fractions.

The convexity of $\dot{W}_H(\dot{\boldsymbol{\varepsilon}}^G)$, however, is broken if the bands are mutually misoriented. To describe the misorientation, we let the misorientation angle between the bands be $2\omega_m$ about an axis given by the unit vector

$$\hat{\mathbf{m}} = (\sin\theta_m \cos\phi_m,\ \sin\theta_m \sin\phi_m,\ \cos\phi_m). \tag{16}$$

The Schmid tensor $\mathbf{m}^s$, for each s of the first band is assumed rotated by an angle $+\omega_m$ relative to the sth Schmid tensor of the original (homogeneously deforming) grain, while that of the second band is assumed rotated by $-\omega_m$, about $\hat{\mathbf{m}}$. The critical resolved shear stress τ_s is, however, assumed to be the same for each s in each band as that in the original grain.

The physical phenomenon idealized by the misorientation ω_m is the misorientation across IDBs that accompany plastic deformation. Hughes *et al.* (1997) found that the average misorientation across IDBs, ω_{av}, scales with grain von Mises strain ϵ_{vM} as

$$\omega_{av} = k_\omega \epsilon_{vM}^{\nu}, \tag{17}$$

where empirical exponent values of $\nu = 0.5$ for cold rolled pure aluminium (Hughes *et al.* 1997) and $\nu = 0.4$ for commercial purity aluminium (Liu *et al.* 2002) have been reported, and $k_\omega (\approx 1^\circ$ for aluminium) is the scaling constant. They also find that misorientation axes corresponding to IDBs are uniformly distributed over all

possible directions. Furthermore, Hughes *et al.* have also found experimentally that the statistical distribution of misorientation angles has a heavy upper tail, i.e. misorientation angles four or five times the average ω_{av} are rare, but do occur.

We thus regard IDBs as *misorientation seeds*. The idea behind the present criterion of grain banding is that of all IDBs, an energetically optimal IDB will be favoured to form a DBB that may, with further deformation, develop large misorientation across itself. Since IDB misorientation axes are uniformly distributed over all possible directions, finding the energetically optimal IDB amounts to finding a misorientation axis, and a misorientation angle (within bounds) at which $\dot{W}_{\mathrm{i}}$ is minimized.

We will now describe the minimization procedure for $\dot{W}_{\mathrm{i}}$. Given $\dot{\boldsymbol{\varepsilon}}^{\mathrm{G}}$, for fixed w, θ_{m}, ϕ_{m} and ω_{m}, different choices of $(\dot{\boldsymbol{\varepsilon}}^{(1)}, \dot{\boldsymbol{\varepsilon}}^{(2)})$ satisfying equation (13) will result in different $\dot{W}_{\mathrm{i}}$ according to equation (14). Appendix A shows that, of all such choices, that choice of $(\dot{\boldsymbol{\varepsilon}}^{(1)}, \dot{\boldsymbol{\varepsilon}}^{(2)})$ satisfying equation (13) will minimize $\dot{W}_{\mathrm{i}}$ which, in addition, satisfies

$$\boldsymbol{\sigma}^{(1)} = \boldsymbol{\sigma}^{(2)}. \tag{18}$$

Since we wish to minimize $\dot{W}_{\mathrm{i}}$, we restrict ourselves to this case only. Then, defining $\boldsymbol{\sigma}^{\mathrm{G}} := \boldsymbol{\sigma}^{(1)} = \boldsymbol{\sigma}^{(2)}$, $\dot{W}_{\mathrm{i}}$ can be written as

$$\begin{aligned}\dot{W}_{\mathrm{i}}(w, \theta_{\mathrm{m}}, \phi_{\mathrm{m}}, \omega_{\mathrm{m}}) &= \boldsymbol{\sigma}^{\mathrm{G}} : [w\dot{\boldsymbol{\varepsilon}}^{(1)} + (1-w)\dot{\boldsymbol{\varepsilon}}^{(2)}] \\ &= \boldsymbol{\sigma}^{\mathrm{G}} : \dot{\boldsymbol{\varepsilon}}^{\mathrm{G}} = w \sum_{s=1}^{S} \tau_s \left| \frac{\boldsymbol{\sigma}^{\mathrm{G}} : \mathbf{m}^{s,(1)}}{\tau^s} \right|^{n+1} \\ &\quad + (1-w) \sum_{s=1}^{S} \tau_s \left| \frac{\boldsymbol{\sigma}^{\mathrm{G}} : \mathbf{m}^{s,(2)}}{\tau^s} \right|^{n+1}. \end{aligned} \tag{19}$$

Here, $\mathbf{m}^{s,(1)}$ and $\mathbf{m}^{s,(2)}$ represent the sth Schmid tensor (equation (3)) of each of the two bands rotated relative to the original grain by $\pm\omega_{\mathrm{m}}$ about $\hat{\mathbf{m}}$.

Let $\dot{W}_{\mathrm{i}}^{*}$ denote the minimum banded power of a grain

$$\dot{W}_{\mathrm{i}}^{*} = \min_{w, \theta_{\mathrm{m}}, \phi_{\mathrm{m}}, \omega_{\mathrm{m}}} \dot{W}_{\mathrm{i}}(w, \theta_{\mathrm{m}}, \phi_{\mathrm{m}}, \omega_{\mathrm{m}}), \tag{20}$$

subject to the constraints equation (13), equation (18) and

$$\begin{aligned} &0 \leq \omega_{\mathrm{m}} \leq r\omega_{\mathrm{av}}, \\ &0 \leq \theta_{\mathrm{m}}, \phi_{\mathrm{m}} \leq \pi. \end{aligned} \tag{21}$$

We implement the minimization of equation (20) using a standard gradient-based constrained optimization package (Spellucci 1998). Although the analytical computation of the gradients $\partial\dot{W}_{\mathrm{i}}/\partial w$, $\partial\dot{W}_{\mathrm{i}}/\partial\theta_{\mathrm{m}}$, $\partial\dot{W}_{\mathrm{i}}/\partial\phi_{\mathrm{m}}$ and $\partial\dot{W}_{\mathrm{i}}/\partial\omega_{\mathrm{m}}$ is tedious, it proves computationally advantageous over numerical differentiation for the gradients.

The first constraint in equation (21) expresses the fact that misorientations across IDBs are usually fairly small, and grow with strain according to equation (17). $r \geq 1$ denotes the factor by which the misorientation angle at band inception is allowed to exceed the average misorientation angle as given by equation (17). As already noted, the upper tail of the misorientation distribution is found to be heavy, and r denotes the ratio of the maximum allowable misorientation to the average misorientation.

The bounds on θ_m and ϕ_m simply restrict the misorientation axis to a half space. They can be narrowed further by accounting for lattice symmetry.

A degenerate minimum, often achieved, arises at $w=0$ or $w=1$. Physically, this corresponds to the situation that $\min \dot{W}_i$ is achieved by rotating the entire grain by ω_m about some misorientation axis $\hat{\mathbf{m}}$. For grains embedded in a polycrystal, we rule out such rotations on physical grounds, and take the banding criterion as having failed in this case. Even in the absence of this degeneracy, we disallow the grain from being dominated by one band. For a fixed $0 \leq c < 0.5$, we take the banding condition as having failed unless $c \leq w \leq 1-c$. We take $c = 0.2$, and thus ensure that the smaller band at least occupies 20% of the grain volume.

Note that homogeneous deformation is one of the states of the banded strain over which minimization is done: it corresponds to $\omega_m = 0$. If the minimum is achieved away from the homogeneous deformation state, and is not degenerate, it implies that banding does indeed lower the plastic power of deformation below that of homogeneous deformation.

In the case of deformation paths such as rolling, which lead to the progressive flattening of grains, it has been argued (see e.g. Hosford (1993, chap. 6)) that the full constraints (FCs) condition, equation (13), may be unrealistic. A better approximation of the imposed deformation, it is argued, is provided by relaxing the shear strain components whose complementary stresses shear the flat surfaces of the grain. Thus, if as shown in figure 3, $\mathbf{n}_{RC}$ denotes the normal to the flat surface of the grain and parallel to the sample coordinate system's 2-direction, the strain rate components $\dot{\epsilon}_3 = \dot{\epsilon}_{12}$ and $\dot{\epsilon}_5 = \dot{\epsilon}_{23}$ are relaxed by writing

$$\begin{aligned} w\dot{\epsilon}_i^{(1)} + (1-w)\dot{\epsilon}_i^{(2)} &= \dot{\epsilon}_i^G, \qquad i = 1, 2, 4, \\ w\sigma_i^{(1)} + (1-w)\sigma_i^{(2)} &= \sigma_i^G, \qquad i = 3, 5, \end{aligned} \tag{22}$$

instead of equation (13). It turns out that equation (18) holds true under the imposed relaxed constraints (RCs) deformation given by equation (22) also, provided $\sigma_3^G = \sigma_5^G = 0$. Thus the minimization in equation (20) is still applicable to RC, although the details of its implementation are different from that in FC.

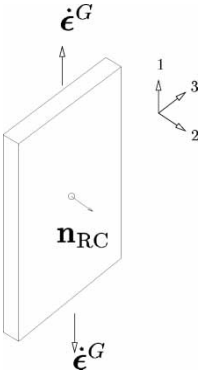

Figure 3. Relaxed constraints are more appropriate to model flat grain deformation than full constraints.

3.2.2. *Accommodation power* ($\dot{W}_b + \dot{W}_c$)

In the case that $\dot{W}_{\mathrm{i}}^{*}$ is attained in a state of banded deformation, the above procedure yields $\dot{\boldsymbol{\varepsilon}}^{(1)}$, $\dot{\boldsymbol{\varepsilon}}^{(2)}$, $\boldsymbol{\sigma}^{(1)} = \boldsymbol{\sigma}^{(2)}$ and w of the DB, and the misorientation axis $\hat{\mathbf{m}}$ and angle ω_{m} of the DBB. DBB orientation, however, is not given by this minimization. Note that, since stress is uniform, equilibrium is fulfilled across every plane in the grain. However, in general, the DB deformations will not be compatible. That is, if $\mathbf{L}^{(1)}$ and $\mathbf{L}^{(2)}$ are DB velocity gradients (from equation (4), where $\dot{\gamma}^{s}$ are given by equation (8)), the condition for compatibility (Hill 1961) is that there exists a vector $\mathbf{a}$ such that

$$\mathbf{L}^{(1)} - \mathbf{L}^{(2)} = \mathbf{a} \otimes \mathbf{n}. \tag{23}$$

This condition is not satisfied in general.

Incompatibility also occurs due to banding at the grain boundary. As shown in figure 2, inhomogeneity in grain bulk deformation may alter its surface profile, leading to incompatibility with neighbouring grains. Thus, although compatible deformation across grain boundaries is guaranteed in a Taylor polycrystal with homogeneously deforming grains, grain boundary accommodation will be needed if banding is allowed.

Following Ashby (1970), we will assume that compatibility is restored by local inhomogeneous deformations close to the DBB and grain boundaries, thereby generating geometrically necessary dislocations (GNDs). We take the energy stored in DBBs to be Chin and Wonsiewicz's $\dot{W}_{\mathrm{b}}$, and the stored energy at the grain boundary to be their $\dot{W}_{\mathrm{c}}$ (see equation (1)). The complexity of the highly inhomogeneous accommodation processes at these boundaries precludes accurate computation of these terms. An order of magnitude estimate is, however, possible and discussed in Appendix B. According to this estimate

$$\dot{W}_{\mathrm{b}} = \kappa_{\mathrm{b}} \frac{N\alpha G b}{D} \|[\mathbf{L}_0]\mathbf{F}_0 \times \mathbf{n}\|, \tag{24}$$

and

$$\dot{W}_{\mathrm{c}} = \frac{N}{2} \frac{\alpha G b \delta_{\mathrm{c}}}{D^2} \|[\mathbf{L}_0]\mathbf{F}_0\|. \tag{25}$$

Here, $[\mathbf{L}_0]$ is the jump in the velocity gradient of the grain parallel to the DBB normal $\mathbf{n}$, and $\mathbf{F}_0$ the deformation gradient of the (hitherto homogeneously deforming) grain at the instant of banding. D is the diameter of the grain, G the shear modulus, b the magnitude of Burgers vector, α a dislocation interaction parameter, and N the number of DBBs. κ_{b} is an unknown factor of the order of one to compensate for the approximations employed in deriving the above expressions, and δ_{c} the thickness of the accommodation layer at the grain boundary.

δ_{c} has been discussed by Meyers and Ashworth (1982). They suggest that δ_{c} may be a function of grain diameter, and suggest the power law dependence: $\delta_{\mathrm{c}} \sim D^{m}$. In a banded grain with N bands, since the smallest dimension of each band is of the order of (D/N), it seems reasonable to take $\delta_{\mathrm{c}} \sim (D/N)^{m}$. For reasons to become clear below equation (30), we assume

$$\delta_{\mathrm{c}} = \kappa_{\mathrm{c}} \left(\frac{D}{D_0 N} \right)^{2}, \tag{26}$$

where D_0 is a reference diameter and κ_c/D_0^2 is a scaling constant. Then, equation (25) becomes

$$\dot{W}_c = \frac{\kappa_c \alpha G b}{2 D_0^2 N} \|[\mathbf{L}_0]\mathbf{F}_0\|. \tag{27}$$

The term $\dot{W}_b$ depends on the orientation of the band interface normal $\mathbf{n}$, while $\dot{W}_c$ does not. We hypothesize that $\mathbf{n}$ is so as to minimize $\dot{W}_b$. This entails a minimization in the two-dimensional space of (θ_n, ϕ_n) if $\mathbf{n}$ were parameterized as

$$\mathbf{n} = [\sin\theta_n \cos\phi_n,\ \sin\theta_n \sin\phi_n,\ \cos\phi_n]^T. \tag{28}$$

So far, N has been left undetermined. Lee and Duggan (1993) suggest that the number of bands will be so as to minimize the total power of accommodation $\dot{W}_b + \dot{W}_c$ at the instant of banding. ($\dot{W}_i$ is independent of N.) Temporarily regarding N as a continuous variable and setting

$$\frac{d(\dot{W}_b + \dot{W}_c)}{dN} = 0 \tag{29}$$

yields

$$N = \sqrt{D}\sqrt{\frac{\kappa_c}{2\kappa_b D_0^2}\frac{\|[\mathbf{L}_0]\mathbf{F}_0\|}{\|[\mathbf{L}_0]\mathbf{F}_0 \times \mathbf{n}\|}}. \tag{30}$$

The square root scaling $N \sim \sqrt{D}$ was derived by Lee *et al.* (1933) using completely different physical arguments, and different expressions for $\dot{W}_b$ and $\dot{W}_c$. Underlying our derivation of this relation is the power law assumption in equation (26). For any powers smaller than $m = 2$, the optimal number of bands would be $N = 0$; for powers larger than $m = 2$, other scaling relations will follow. Thus the presently chosen $m = 2$ represents the smallest exponent in equation (26) for which banding is possible. To render N an integer, we round down the value calculated using equation (30). The banding condition is taken to fail if $N = 0$.

With respect to N, the present model follows the viewpoint of Lee *et al.* (1993) in assuming that N is determined at the instant of banding, and does not evolve with further deformation. In contrast, the model of Ortiz *et al.* (2000) subdivides grains into $N = 2$ bands, these bands being allowed to divide with further deformation. However, it is easy to see a synthesis of these two viewpoints, with grains banding into N (not necessarily equal to two) bands according to Lee *et al.*'s (1993) idea, and these bands refining further according to the model of Ortiz *et al.* (2000).

In summary, the banding condition involves performing the minimization given by equation (20). If the minimum is achieved in a non-degenerate state of inhomogeneous deformation, and the reduction in deformation power exceeds the power of accommodation, equations (24) and (25), the grain is theorized to band. If any of these tests fail, the grain is assumed to continue deforming homogeneously. The deformation banding test is carried out at every strain increment in our incremental implementation of polycrystal plasticity.

3.3. *Deformation of a banded grain*

The preceding section 3.2 was concerned with a criterion for the formation of DB. The further deformation of a grain, once banded, will be discussed here.

According to the Taylor theory of homogeneously deforming grains, the activation of slip systems for a given imposed deformation occurs so as to minimize the plastic power $\dot{W}_{\mathrm{H}}$ in equation (12) (Chin and Mammel 1969). This notion is directly extensible to the inhomogeneous deformation case: the inhomogeneous plastic power given by equation (14) should be minimized subject to the constraint equation (13) that the imposed deformation on the grain be satisfied. As already discussed, this minimum occurs when equation (18) is satisfied. Thus, explicitly, given $\dot{\boldsymbol{\varepsilon}}^{\mathrm{G}}$, the 20 algebraic equations to be solved for determining the deformation in a banded grain as described by the 20 components of $\dot{\boldsymbol{\varepsilon}}^{(1)}$, $\dot{\boldsymbol{\varepsilon}}^{(2)}$, $\boldsymbol{\sigma}^{(1)}$ and $\boldsymbol{\sigma}^{(2)}$ are

$$\begin{aligned} \dot{\boldsymbol{\varepsilon}}^{\mathrm{G}} &= w\dot{\boldsymbol{\varepsilon}}^{(1)} + (1-w)\dot{\boldsymbol{\varepsilon}}^{(2)}, \\ \boldsymbol{\sigma}^{(1)} &= \boldsymbol{\sigma}^{(2)}, \quad \text{and} \\ \dot{\boldsymbol{\varepsilon}}^{(i)} &= \sum_{s=1}^{S} \mathbf{m}^{s,(i)} \left| \frac{\boldsymbol{\sigma}^{(i)} : \mathbf{m}^{s,(i)}}{\tau^{s,(i)}} \right|^{n} \operatorname{sign}(\boldsymbol{\sigma}^{(i)} : \mathbf{m}^{s,(i)}), \qquad i = 1, 2. \end{aligned} \tag{31}$$

Here, $\mathbf{m}^{s,(1)}$ and $\mathbf{m}^{s,(2)}$ refer to the Schmid tensors of the sth slip system in the first and second band, respectively, and $\tau^{s,(1)}$ and $\tau^{s,(2)}$ to their critical resolved shear stresses. In minimizing the power of deformation, the power of accommodation of incompatibly deforming bands is taken to be negligible in comparison with the plastic power.

Once a grain bands, we assume that the volume fraction of each band, w, and $1-w$ are fixed thereafter, i.e. the DBB has no mobility relative to the bands. As for the orientation of the DBB, we assume that it rotates with the grain shape (not lattice). That is, if the band forms with normal $\mathbf{n}_0$ when the grain deformation gradient is $\mathbf{F}_0$, the normal $\mathbf{n}$ when the deformation gradient is $\mathbf{F}$ will be

$$\mathbf{n} = \mathbf{F}_0^{\mathrm{T}}\mathbf{F}^{-\mathrm{T}}\mathbf{n}_0 / \|\mathbf{F}_0^{\mathrm{T}}\mathbf{F}^{-\mathrm{T}}\mathbf{n}_0\|. \tag{32}$$

To see this, consider two vectors $\mathbf{a}$ and $\mathbf{b}$ in the plane of the band interface (i.e. parallel to the DBB) at the instant of banding when the grain deformation gradient is $\mathbf{F}_0$. $\mathbf{n}_0$ is thus parallel to $\mathbf{a} \times \mathbf{b}$. The deformation gradient of the transformation from this state to the final deformation gradient of $\mathbf{F}$ is $\mathbf{F}_0^{-1}\mathbf{F}$. Under this transformation, $\mathbf{a} \times \mathbf{b}$ maps to $(\mathbf{F}_0^{-1}\mathbf{F}\mathbf{a}) \times (\mathbf{F}_0^{-1}\mathbf{F}\mathbf{b})$. Now, using the identity (Gurtin 1981, p. 53) $\mathbf{S}\mathbf{a} \times \mathbf{S}\mathbf{b} = \det(\mathbf{S})\mathbf{S}^{-\mathrm{T}}(\mathbf{a} \times \mathbf{b})$, it is seen that the unit normal to the banded plane is the unit vector parallel to $\mathbf{F}_0^{\mathrm{T}}\mathbf{F}^{-\mathrm{T}}(\mathbf{a} \times \mathbf{b})$.

The preceding assumptions of (1) continuing deformation of a banded grain so as to minimize its plastic power of deformation, (2) the immobility of DBBs relative to DBs, and (3) the rotation of DBBs with the shape of the grain, can only be tested by comparing the predictions of this theory with experiment. However, the more fundamental assumption of the theory that large misorientations develop across favourably oriented DBBs with slight misorientations is based on the experimental observations of Cizek *et al.* (1995) and Hughes and Hansen (1997).

§ 4. Results and discussion

We use the present theory to simulate plastic deformation under uniaxial tension, uniaxial compression, and plane strain rolling, of a 200 grain aggregate, whose orientations are initially random and uniformly distributed over all possible orientations. Taylor polycrystal approximation is assumed, viz. the macroscopically

imposed deformation is experienced by each grain. This ensures compatibility across grain boundaries, but, in general, results in the violation of equilibrium across them.

Our polycrystal plasticity code implements an incremental formulation of rigid-plastic crystal plasticity obeying the viscoplastic constitutive equation (9). The entire deformation is divided into small steps of strain increments, at each of which the shear rates $\dot{\gamma}^s$ of each slip system are calculated according to equation (9), and the orientation of each grain or band and hardness of slip systems within each grain or band is updated. These updates are discussed by Kocks *et al*. (1998, chap. 8). The Voce hardening law as extended by Tomé *et al*. (1984) to account for non-saturation of flow stresses (stage IV hardening) is assumed with no latent hardening of slip systems due to the activity of other slip systems. If τ_s^c is the critical resolved shear stress in slip system s, and the accumulated strain in that system is Γ, the hardening law relates them as

$$\tau_s^c(\Gamma) = \tau_0 + (\tau_1 + \theta_1\Gamma)[1 - \exp(-\theta_0\Gamma/\tau_1)]. \tag{33}$$

τ_0, τ_1, θ_0 and θ_1 are material parameters. At each step, the banding condition discussed in section 3.2 is checked, if the grain is not already banded. If it is banded, it is not allowed to band further. The procedure of section 3.3 is used to compute the stress and slip rates of the S slip systems in each band.

We will now apply the present theory of inhomogeneous grain deformation to fcc aluminium and bcc α-iron subjected to monotonic tension, compression and plane strain rolling deformations. Aluminium grains are assumed to deform solely by $\langle 110\rangle(111)$ slip and α-iron grains solely by $\langle 111\rangle(110)$ slip. In mild steel, Duggan *et al*. (1998) find it important to consider both $\langle 111\rangle(110)$ and $\langle 112\rangle(111)$ slip, and to adjust the critical resolved shear stress ratio of the two systems appropriately to capture the cold rolling texture. However, for reasons of simplicity in interpreting the results of the model, especially in view of the difficulty of disentangling the contributions to texture evolution of deformation banding and enhanced latent hardening in a $\langle 111\rangle(110) + \langle 112\rangle(111)$ slipping grain, we limit our α-iron model grains to $\langle 111\rangle(110)$ slip only. We will see below (figure 7) that this assumption notwithstanding, the present model succeeds in capturing the banding behaviour of α-iron. Also, in comparing bcc and fcc banding behaviour, ideally data at the same homologous temperature will be considered. However, only room temperature experimental data is presently available for both metals, and this will be used.

In discussing tension and compression below, the sample coordinate system is such that its '1' axis is along the tensile (TA) or compressive axis (CA). In discussing rolling, the sample '1'-axis is along the rolling direction (RD), the '2'-axis along the transverse direction (TD) and the '3'-axis along the normal direction (ND).

Experimental tensile stress–strain curves for the two metals under consideration, large-grained (400 μm average grain diameter) aluminium and α-iron, have been reported by Sil and Varma (1993) and Tjerkstra (1961), respectively. In the single crystal aluminium specimen of Basson and Driver (2000), the typical DB width is of the order of 40 μm, so one may expect about 10 DB to form in the grains studied by Sil and Varma, in a way reasonably undisturbed by flow field inhomogeneities due to grain–grain interactions, which predominate in fine-grained polycrystals (Dawson *et al*. 2000). Also, only large grains can accommodate large dislocation structures, the importance of which was discussed in section 1 in connection with Winther's observation.

Table 1. The model parameters as fit to the tensile experimental stress–strain curve for aluminium and α-iron.

Parameter	Ref.	Al	α-Fe
n	Equation (9)	20	20
k_ω (deg)	Equation (17)	1	1
r	Equation (21)	4	4
c	Equation (21)	0.2	0.2
D (m)	Equation (30)	4×10^{-4}	4×10^{-4}
κ_b	Equation (48)	0.025	0.025
$\kappa_c/D_0^2(\mathrm{m}^{-1})$	Equation (52)	10^3	10^3
$Gb(\mathrm{MPa\,m}^{-1})$	Various	1.25×10^{-5}	2.31×10^{-5}
θ_0(MPa)	Equation (33)	30.0	170.0
θ_1(MPa)	Equation (33)	0.5	3.0
τ_0(MPa)	Equation (33)	3.5	18.0
τ_1(MPa)	Equation (33)	19.0	87.0

The experimental stress–strain curves for aluminium and α-iron allow us to calibrate the deformation banding model. Table 1 lists the parameters thus fit. The values of k_ω and r were approximated for aluminium from the data of Hughes *et al.* (1997), and lacking such information for iron, the same values are used. c was discussed below equation (21). The values of κ_b and κ_c/D_0^2 were chosen small enough that banding will be possible, and with such a ratio that equation (30) will result in about 10 bands in banding grains. Furthermore, we require that κ_c/D_0^2 be such that equation (26) yields a reasonable value for δ_c: with $N = 10$, $D = 400 \times 10^{-6}\,\mathrm{m}$, the present value of $\kappa_c/D_0^2 = 1000\,\mathrm{m}^{-1}$ results in $\delta_c = 1.6\,\mu\mathrm{m}$, which seems plausible. These estimates can be expected to be correct only in their orders of magnitude, and not in their numerical value. Lacking any motivation for distinction in their values between aluminium and iron, we take both the same. Keeping the above deformation banding parameters fixed, the hardening parameters of equation (33) were adjusted until good agreement was obtained between the calculated and experimental curves.

The exact numerical value of these parameters is unimportant. It seldom happens that the banding condition fails because $\dot{W}_H - \dot{W}_i^* < \dot{W}_b + \dot{W}_c$ in equation (1). In fact, given our parameter set, the right side of this inequality hardly ever exceeds 10% of the left side, whenever the left side is positive. In this observation, the present model agrees with Lee *et al.* (1995), who suggest simply taking $\dot{W}_b + \dot{W}_c = 0.05\dot{W}_i$ in equation (1). A far more common reason that a simulation grain does not band is that $\min \dot{W}_i$ is achieved at $w \leq c$, or $w \geq 1 - c$ (see text below equation (21)), or $N = 0$ (see text below equation (30)).

Figure 4 shows the good fit between the stress–strain curves calculated using these parameters and the experimental data in uniaxial tension. The experimental data go only up to $\epsilon_{11} = 0.25$; the calculations have been carried out to twice that strain. Also shown in this figure for comparison are the calculated stress–strain curves in tension obtained by suppressing banding. Note that the polycrystal material that allows for banding is the softer one in both metals, as expected from the energetic basis of computing the deformation of banded grains. It is reassuring that the difference between the banded and homogeneous response of a polycrystal is not very big; classical models are adequate to predict mechanical response when the grain substructure is not of interest.

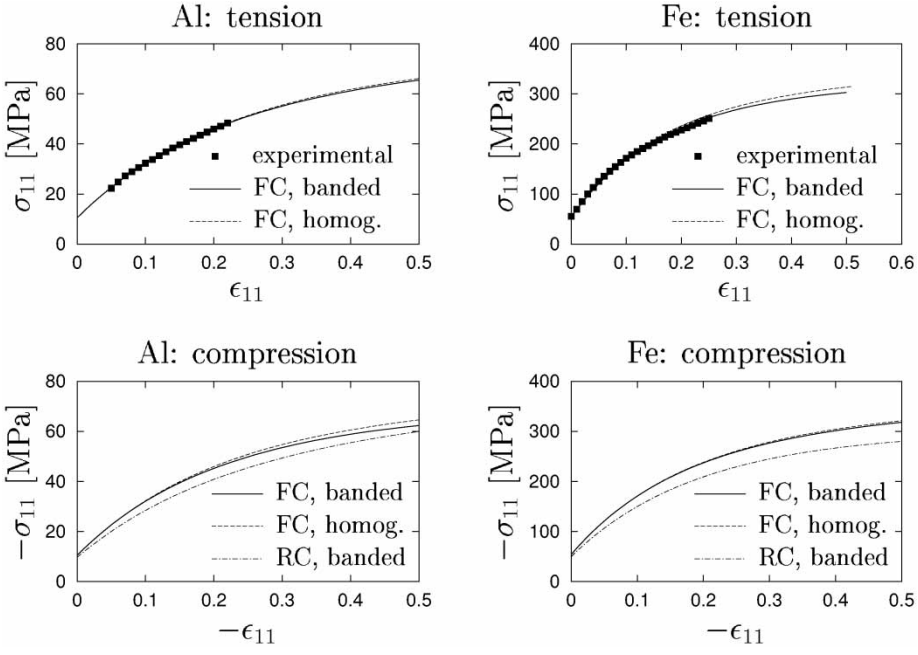

Figure 4. Row 1: fits of the experimental tensile curve for aluminium and α-iron to the calculated curves assuming deformation banding obtained using the parameters in table 1. Also shown are the curves obtained using these parameters, while suppressing deformation banding. Row 2: calculated stress–strain curve under compression in both metals using the same parameters.

However, allowing for banding makes far less difference during tension of fcc aluminium (the flow stress gap between the banding and homogeneous polycrystals is only 0.65 MPa, or 1% at $\epsilon_{11} = 0.5$) than of bcc iron (the gap is 12.2 MPa, or 4%). Figure 4 also shows the calculated compression stress–strain curve for polycrystals of both metals with both banded and homogeneous deformation. In compression, the importance of microstructure reverses between aluminium (the gap is 2.29 MPa, or 6% at $\epsilon_{11} = 0.5$) and iron (the gap is 3.06 MPa or 1.5% at $\epsilon_{11} = 0.5$). Since in compression and rolling (and *not* in tension), as the grains become flatter with deformation, relaxed constraints (RCs), rather than full constraints (FCs), may be a better approximation of the deformation imposed on a grain, stress–strain curves assuming RC and allowing for banding are also shown. As can be seen, the RC prediction is softer than the FC prediction. Also, the RC curve appears poised to intersect the FC curve in the case of aluminium, but not in the case of iron.

The reversal in the importance of banding between tension and compression, and the contrasting behaviour of the difference between FC and RC curves, can be explained by studying the predicted microstructure in each metal. Figure 5 shows the calculated misorientation distribution across DBBs at $|\epsilon_{11}| = 0.5$ in tension, compression and rolling. As seen, the frequency of grains with large misorientations is larger in compression than in tension in fcc aluminium and vice versa in bcc steel. Thus, banded grains deform more similar to homogeneous ones in tension in fcc aluminium than during compression, and vice versa in bcc iron. This explains the smaller influence of banding on flow response during tension than compression in aluminium, and the opposite situation in iron.

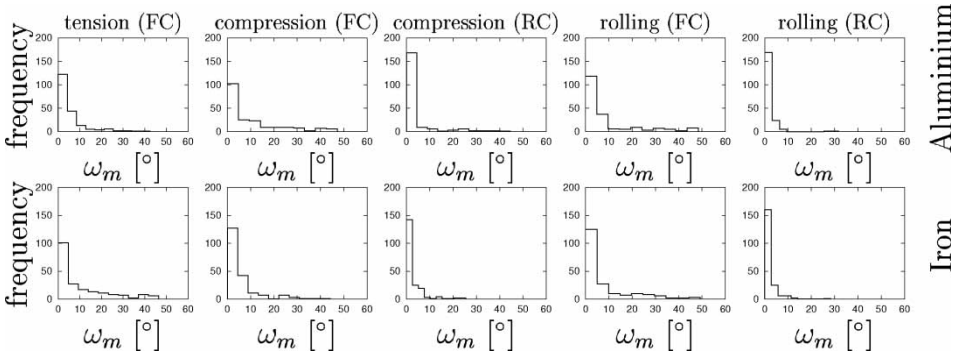

Figure 5. Histograms of the distribution of the computed misorientation between deformation bands at $|\epsilon_{11}| = 0.5$, after tension, compression and rolling under FC and RC constraint conditions. The first row is for aluminium, and the second for α-iron. Both the aluminium and α-iron model polycrystals consist of 200 grains.

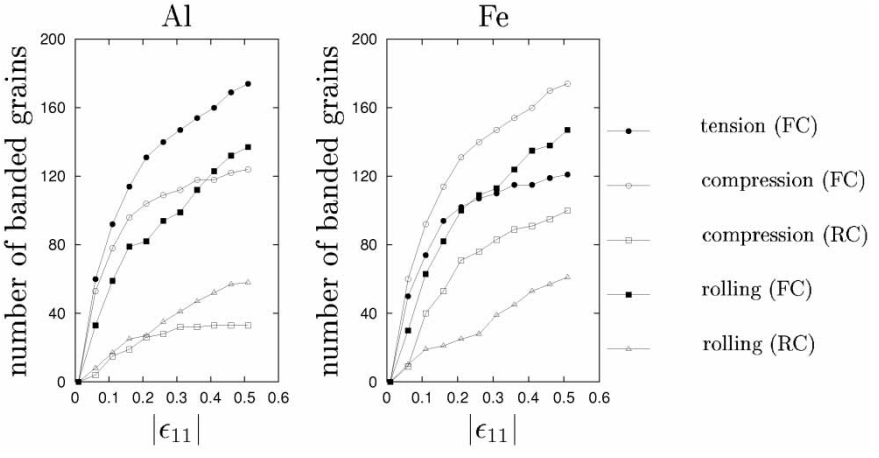

Figure 6. Progress of banding during simulated deformation. Both the aluminium and α-iron model polycrystals consist of 200 grains.

Figure 6 shows the progress of banding in the polycrystal with deformation. The number of grains banding during RC deformation (both in compression and rolling) is smaller than that in FC deformation. This seems reasonable, for if a grain is able to relax its stresses by means of RC, it should have a smaller tendency to band, as banding is simply another means of relaxing components of the stress. The tendency to band under RC is, however, greater in iron than in aluminium. This suggests a reason why the FC and RC compression flow stress curves in aluminium tend toward each other, while those of iron do not (figure 4). While the RC aluminium curve allowing for banding is initially softer than the FC curve, too few grains band in the RC polycrystal, which results in its becoming harder relative to the FC polycrystal after further deformation. Although in iron too, the number of bands formed by the RC polycrystal in compression is fewer than in the FC polycrystal, this number is larger than in aluminium, and seems to lead to an increasing divergence between the RC and FC iron compression curves in figure 4.

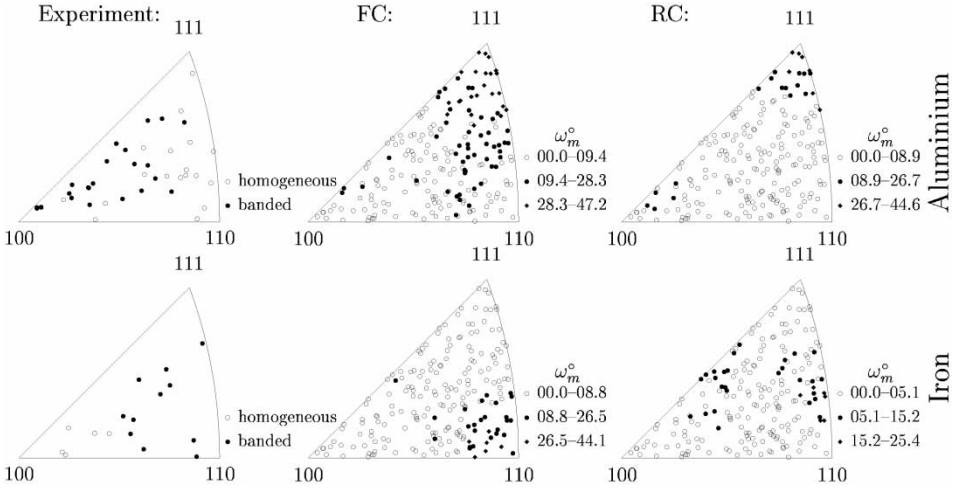

Figure 7. Dependence of misorientation after compression to $\epsilon_{11} = -0.5$ on initial grain orientation. Dots indicate initial (before compression) grain orientation, and the dot shape indicates its misorientation after compression. The rows correspond to aluminium and iron, respectively. First column: inverse compression pole figures experimentally observed by Barrett and Levenson (aluminium), and Barrett (iron). Open symbols denote poles with small misorientation and solid symbols poles with large misorientations. Second column: calculated inverse pole figure assuming FC. Third column: calculated inverse pole figure assuming RC. Open symbols in columns 2 and 3 denote calculated poles with no or small misorientation (less than 20% of the maximum observed misorientation); solid symbols denote the rest of the poles.

In figure 7, we have reproduced the experimental observations of Barret and Levenson (1940) in pure aluminium, and of Barrett (1939) in mild steel depleted of carbon. It shows the initial orientation of grains that did or did not develop bands after nominally uniaxial compression: compression between lubricated plates to $\epsilon_{11} = -1.89$, followed by 'compression rolling' to varying further reductions in the case of aluminium. In the case of mild steel, Barrett's experimental results were obtained on single crystals.

The mechanical response of Barrett's and Barrett and Levenson's materials was not published. As an approximation, therefore, we assume that their material also approximately flows as the experimental data in figure 4. These data, however, only go up to $\epsilon_{11} = 0.25$, giving little indication of the flow response in stage IV, which will be of importance at the extremely high deformations imposed experimentally by Barrett and Levenson. Furthermore, the experimental data presented for iron corresponds to single crystals compressed to a range of reductions. Thus, at best, one can expect to qualitatively compare the predictions of the present theory with this experimental data. We therefore simulate FC and RC compression only to $\epsilon_{11} = -0.5$, and plot the initial orientation of each grain in the inverse pole figures of figure 7 for aluminium and iron, with a symbol that denotes the misorientation across the DBB in each banded grain.

In the case of aluminium, both FC and RC simulations of deformation suggest that the grains that band have initial orientations close to the [111] corner. These bands must therefore be forming early in the deformation, since orientations near [111] move toward [110] quite rapidly (see also figure 12). The FC calculation

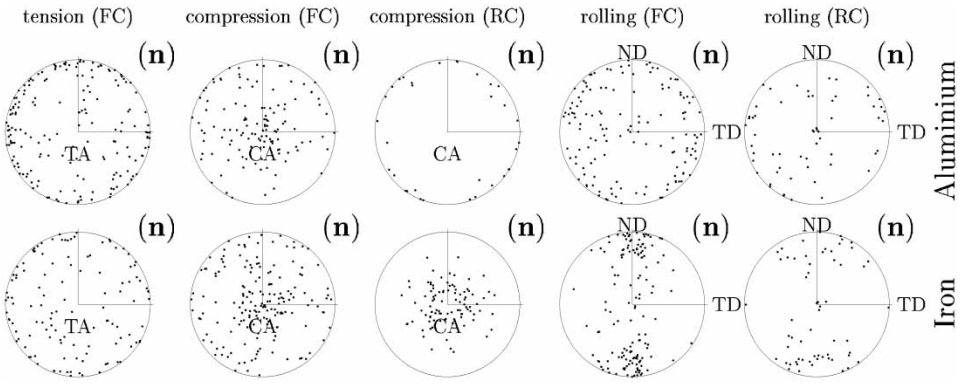

Figure 8. Calculated pole figures (equal area projection, no symmetrization applied) of the orientation of DBB normals $\mathbf{n}$ after $|\epsilon_{11}| = 0.5$ deformation in tension (only FC), compression and rolling (both FC and RC calculations). TA denotes the tensile axis, CA the compression axis, RD the rolling direction, TD the transverse direction and ND the normal direction. Only grains that band are represented by dots in this figure.

predicts more banded grains than RC, spilling into the main part of the triangle. Some banding also takes place near the [100] corner, and none at all near the [110] corner of the pole figure triangle. Barrett and Levenson also observe many banded grains in the main part of the triangle, and near the [100] corner, but none near [110]. The main discrepancy between the FC predictions and the experimental observation lies at the [111] corner. Here, however, Barrett and Levenson have but one data point, and three of the nearest four data points show banding grains. For this reason, we are doubtful that there actually is a discrepancy between experiment and calculation here too.

In the case of iron, the FC and RC computations show qualitative distinctions among themselves. FC bands are concentrated near the [110] corner, while RC bands form near the [110]–[111] and [111]–[100] lines. Realizing that the actual constraint experienced by the grain lies somewhere in between the extremes defined by FC, and RC, one can qualitatively view the actual banding pattern in the polycrystal as lying in between the two predictions shown. The experimental observation of Barrett qualitatively agrees with this. It shows no banding near the [100] corner, although again the [111] corner is uncertain. Banding does occur at the [110] corner and spills into the main part of the triangle.

Figure 8 presents the orientation of DBB normals on pole figures after deformation to strain $|\epsilon_{11}| = 0.5$ in tension, compression, and rolling. As is seen, there is a clear tendency of DBB normals away from the loading axis in tension, and toward the loading axis in compression, both in aluminium and α-iron. This is a consequence of the assumption that DBB orientation follows the deformation of the grain as a whole (equation (32)). The shape change and normal $\mathbf{n}_1$ reorientation is depicted schematically in figure 9. The exceptionally oriented DBB, labelled $\mathbf{n}_2$ in figure 9, with normals parallel to the loading axis in tension, and perpendicular to it in compression, form close to that orientation at the instant of banding, and are not reoriented significantly with grain deformation.

The orientations of the DBB normals after compression, calculated using RC, appear qualitatively different in fcc aluminium and bcc iron than those calculated

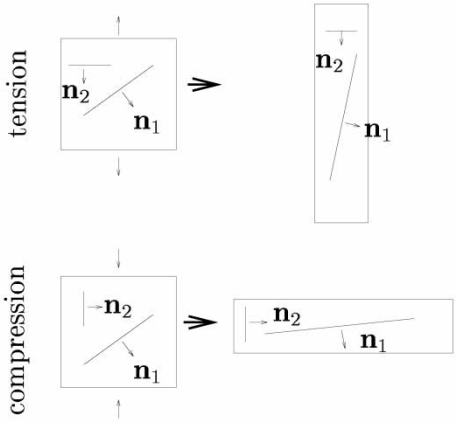

Figure 9. Schematic diagram to explain the observed orientation of DBB normals **n**.

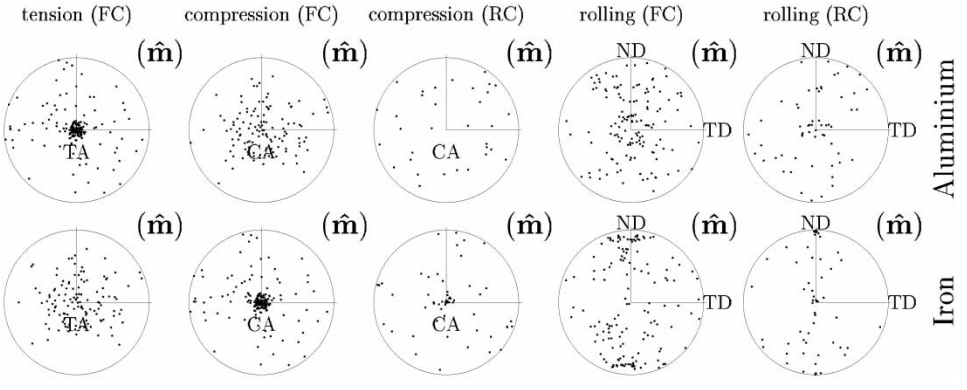

Figure 10. Calculated pole figures (equal area projection) of the orientation of DBB misorientation axes $\hat{\mathbf{m}}$ after $|\epsilon_{11}| = 0.5$ deformation in tension (only FC), compression and rolling (both FC and RC calculations). TA denotes the tensile axis, CA the compression axis, RD the rolling direction, TD the transverse direction and ND the normal direction. Only grains that band are represented by dots in this figure.

using FC. This is because aluminium grains that would have banded with normals not perpendicular to the compression axis under FC, do not band at all under RC. This suggests that RC deformation suffices to adequately relax the stress in these grains, thereby obviating deformation banding. However, in the case of iron, it is the complementary set of grains, those with normals not perpendicular to the compression axis, that do band.

After rolling in both aluminium and iron, there is a definite tendency of the DBB normal orientation away from the rolling direction, in agreement with the experimental observations of Lee and Duggan (1993). In FC rolled aluminium, the normal is approximately uniformly distributed perpendicular to the RD; however, there is a clear propensity for the normal to be parallel to the ND in the case of rolled iron. These tendencies persist in RC rolled aluminium and iron, although fewer grains band under RC.

We next turn toward misorientation axes across DBB shown in figure 10. In FC tension and compression, both in aluminium and iron, a clear tendency of the

misorientation axis toward the loading axis can be seen. This tendency is not so clear in RC compression, but it appears plausible that, with continued deformation, the misorientation axes will rotate parallel to the loading axis even in this case. Taken together with the previous observation of DBB normal orientations, this implies that the tensile DBB in both metals have a predominantly 'tilt' character, while the compressive DBB have a predominantly 'twist' character.

In both aluminium and iron, subjected to either FC or RC plane strain rolling, there is a pronounced tendency of the DBB misorientation axis away from the transverse direction (TD). This conflicts with the experimental observations of Liu and Hansen (1998) and Liu *et al.* (2000), who experimentally studied rolling of unstable cube-oriented ((001)/[100]) single aluminium crystals and found a clear preference for rotation about the TD of deformation bands. Li *et al.* (2004) found the same in unstable (001)/[110] Al–1% Mn. During channel-die compression, Driver and co-workers (Akef and Driver 1991, Basson and Driver 2000) also observed the same.

As discussed by Liu *et al.* (2000), rotation about TD under plane strain deformation will increase the power of deformation, and explains why the present model does not predict this rotation. Liu *et al.* also hypothesized that, in rolling experiments, a shear component due to geometric and frictional effects previously studied by Lee and Duggan (1991) may be causing the rotations about TD. Lee and Duggan (1991) have quantified the requisite magnitude of the shear component to be about 1.5 times the rolling strain to yield the correct textures. Figure 11 shows the effect of this shear component on the orientation of the misorientation axis in (001)/[100] and (001)/[110] aluminium crystals at $\epsilon_{11} = 0.5$. $\mathbf{L}$ here denotes the velocity gradient, and its matrix representation given in the figure corresponds to the coordinate axes described on p. 16. Clearly, the misorientation axis of the cube-oriented crystal, which under plane strain is nearly parallel to the RD, is redirected along TD in the presence of the shear component. The reorientation due to shear of the (001)/[110] orientation is also very nearly parallel to the TD. It should also be mentioned that, although these special orientations show rotation of their bands about the TD, the majority of the (initially randomly oriented) grains continue to rotate about an axis nearly perpendicular to the TD regardless of the imposed shear

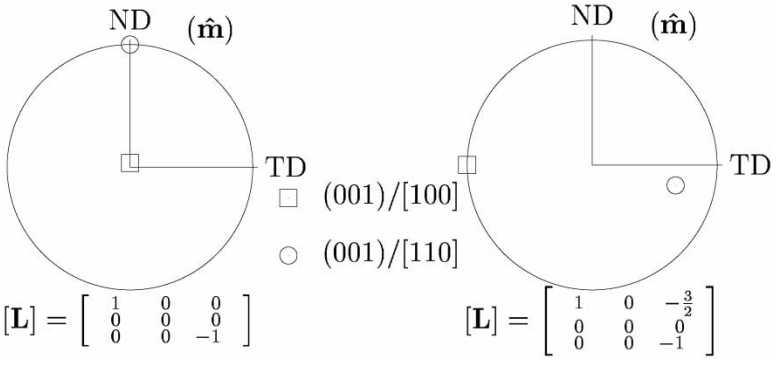

Figure 11. Computed reorientation of the misorientation axis in initially cube oriented (001)/[100] and (001)/[110] oriented single crystals without, and with the shear caused by geometry and friction effects during rolling. Experimentally, the misorientation axis is known to be parallel to TD for these orientations.

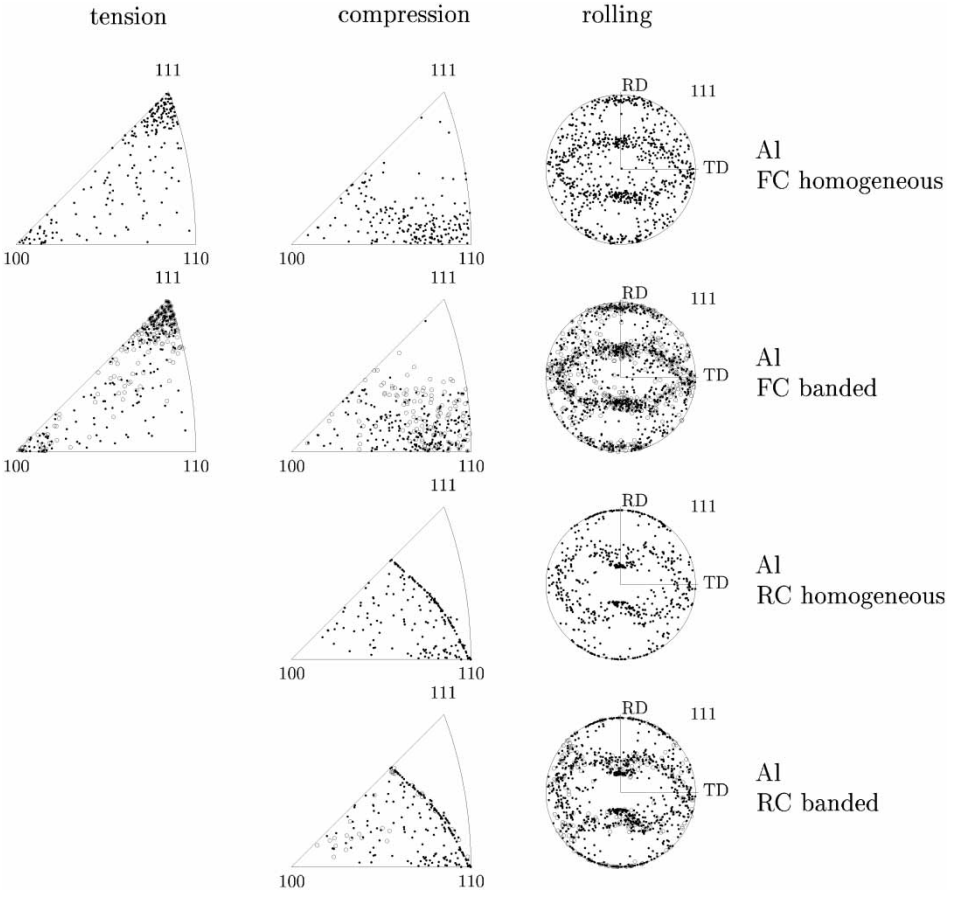

Figure 12. Inverse (tension and compression), and 111 direct pole figures (rolling) for aluminium after strain $|\epsilon_{11}| = 0.5$. The columns correspond to the different loadings as indicated. The rows correspond to FC and RC simulations with or without banding, as indicated. Since RC approximates tension poorly, that calculation is omitted. Open circles: bands with $0 \leq w < 0.5$; dots: bands with $0.5 \leq w \leq 1$.

component $L_{13} = -1.5$; the misorientation axis pole figure under this condition of 200 aluminium grains looks similar to that of the iron polycrystal under FC rolling in figure 10.

Although the frictional and geometric effects considered by Lee and Duggan do not apply to the channel-die experiments of Driver and co-workers, we suspect that here too, the observed misorientation axis is due to an uncharacterized experimental condition. It is known (Humphreys and Ardakani 1994) that slight differences in the material constitution or initial orientation of the crystals can cause qualitative differences in the banding behaviour.

Figures 12 and 13 show the calculated texture developed during tension, compression, and rolling in aluminium and iron, respectively, under three different deformation assumptions: FC and RC, with and without allowing grain banding. As is to be expected, the RC and FC pole figures are qualitatively different. However, banding does not introduce any noticeable qualitative change in the pole figures.

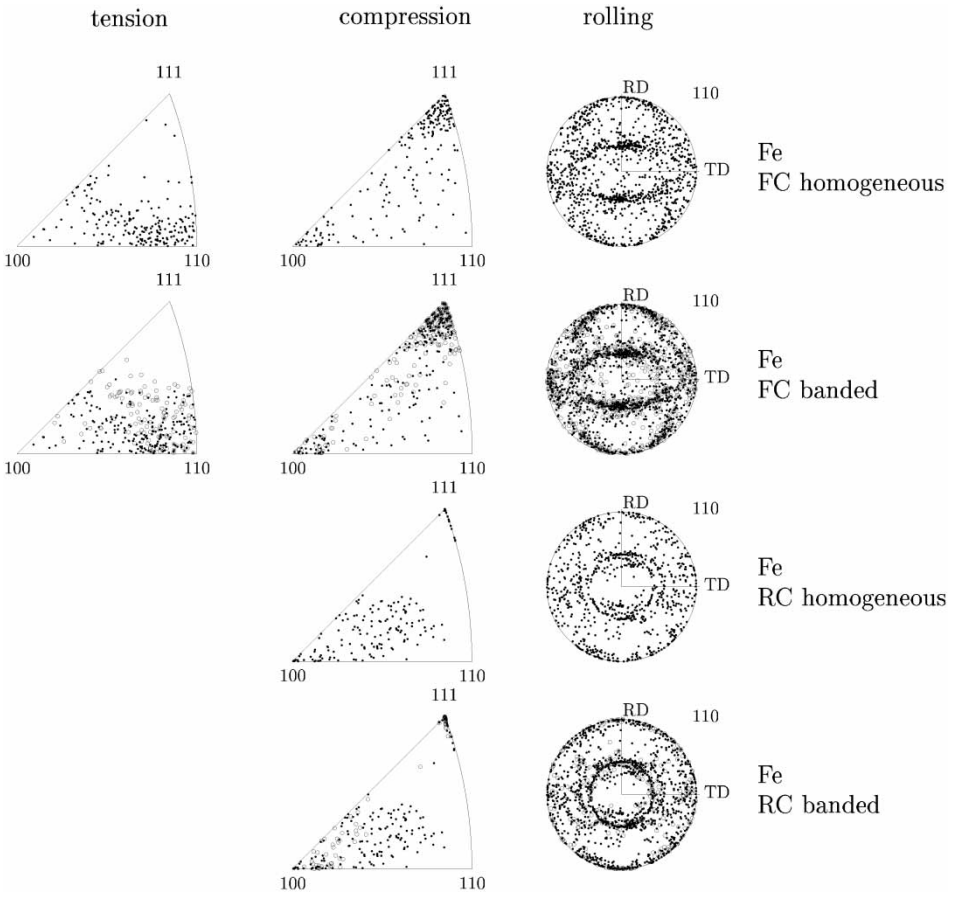

Figure 13. Inverse (tension and compression), and 110 direct pole figures (rolling) for iron after strain $|\epsilon_{11}| = 0.5$. The columns correspond to the different loadings as indicated. The rows correspond to FC and RC simulations with or without banding, as indicated. Since RC approximates tension poorly, that calculation is omitted. Open circles: bands with $0 \leq w < 0.5$; dots: bands with $0.5 \leq w \leq 1$.

It can be seen, however, by comparing intensities, that banding does make the pole figures less sharp. Another point to notice is that there is no systematic separation between heavy and light bands during deformation: both move statistically similarly through orientation space.

Deformation banding lowers the number of active slip systems in banded grains. To quantify the reduction, following Kocks *et al.* (1998, chap. 11), we define the average number of active systems per grain, $\langle n_{\text{active}} \rangle$ as

$$\langle n_{\text{active}} \rangle = \frac{\sum_g n_{\text{active},g} V_g}{\sum_g V_g}, \tag{34}$$

where the summations run over all the bands and grains in the polycrystal. The volume fraction of the band or grain relative to the polycrystal is denoted by V_g, and its total slip rate, $\dot{\Gamma}_g = \sum_s |\dot{\gamma}^s(g)|$. $n_{\text{active},g}$ is the number of *active* slip systems in grain or band g, where a slip system is taken to be active if its slip rate exceeds 5%

Table 2. Average number of active slip systems, $\langle n_{\text{active}} \rangle$ at strain $|\epsilon_{11}| = 0.5$ under the different loading conditions, and different constraints. Note that for a viscoplastic grain (equation (9)), $\langle n_{\text{active}} \rangle$ values in excess of 5 are permissible.

		Aluminium		Iron	
Loading		Banded	Not banded	Banded	Not banded
FC	Tens	5.819	6.214	5.926	7.255
	Comp	5.958	7.257	5.812	6.214
	Roll	4.576	5.403	4.515	5.393
RC	Comp	4.542	4.599	5.265	5.266
	Roll	4.115	4.131	4.226	4.272

of the maximum slip rate in that grain or band. Table 2 lists $\langle n_{\text{active}} \rangle$ under various deformation conditions applied to both aluminium and iron under both FC and RC constraints. It is plainly seen that the reduction in $\langle n_{\text{active}} \rangle$ is larger under FC than under RC for both metals, both because fewer grains band under RC, and because relaxation of constraints acts as an alternative mechanism to lower the plastic power of deformation. Thus, on the basis of its physical hypotheses, the present theory lowers $\langle n_{\text{active}} \rangle$, and hence latent hardening.

§ 5. Conclusions and future work

A theory of inhomogeneous grain deformation has been developed, and used to model deformation banding. According to this theory, deformation bands are initiated at a favourably oriented IDB and develop so as to minimize the plastic power of grain deformation. The banding criterion is dominated by minimization of plastic deformation power, with the accommodation power at band and grain boundaries playing a far lesser role. The model predicts a number of microstructural features of grains in plastically deforming aluminium and α-iron. Comparison with experimental data has been attempted, where such data is available. Experimentally, the formation and evolution of deformation bands can be very sensitive to material and experimental conditions; the large variability in the results of nominally identical loading conditions on nominally identical materials (see e.g. Liu and Hansen (1998, section 4(b)) makes quantitative comparisons between theory and experiment difficult. At best, therefore, only qualitative comparisons are presently possible. Such comparisons are favourable.

The present theory of deformation banding fundamentally differs from that of Lee and Duggan, and Ortiz and co-workers in that an explicit mechanism is proposed here for the initiation of deformation bands from misorientations seeded by IDBs. The latent hardening assumption is not essential for our grains to band; in fact, the banding decision is an instantaneous one based on the present state of the grain as represented by the critical resolved shear stresses of all its slip systems, average grain orientation, and the imposed loading. The present theory, however, reduces the number of active slip systems in each band from that in a grain; in this sense, it reduces latent hardening of the grain as a consequence of its physical hypotheses. Also, the deformation banding criterion does not hinge on rate sensitivity of the grain's constitutive law.

Several extensions of the present theory are possible; four of them are as follows. Firstly, the two different constraining schemes investigated in the present work (FC and RC) represent limiting cases of the actual constraint experienced by the

grain. The self-consistent scheme (Lebensolhn and Tomé 1993) represents a better intermediate approximation of the grain constraints in a polycrystal, and the banding theory, incorporated in the self-consistent framework, should give intermediate results. Here we choose not to pursue the self-consistent model to better isolate the effect of deformation and orientation on banding behaviour of a grain. The same can be said of latent hardening: introducing it in the present calculations would make it harder to interpret our results. Secondly, the present theory allows at most one set of parallel bands to form in each grain. In reality, secondary and tertiary bands are observed (Kulkarni and Kuhlmann-Wilsdorf 1998), which are still many times as big as the mean free path of individual dislocations. Such banding could be permitted. Thirdly, once banded, grains in the present model deform as a composite grain as described in section 3.3. In reality, though, after a certain deformation, bands 'release' and deform as independent new grains (Duggan and Lee 1996). Such a release condition may be effected when a threshold misorientation is achieved. Finally, we believe the present model can be adapted to simulate martensitic or deformation twinning transformations. Both transformations concentrate shears within bands in grains.

Acknowledgements

This research was funded by DOE, Office of Science, Office of Basic Energy Sciences. We thank Dr. R. J. McCabe for helpful criticism of this manuscript.

APPENDIX A

Minimizing plastic power of a banded grain

Here we show that to minimize the plastic power of a banded grain

$$\dot{W}_{\mathrm{i}} = w \sum_{s=1}^{S} \tau_s \left| \frac{\boldsymbol{\sigma}^{(1)} : \mathbf{m}^{s,(1)}}{\tau^s} \right|^{n+1} + (1-w) \sum_{s=1}^{S} \tau_s \left| \frac{\boldsymbol{\sigma}^{(2)} : \mathbf{m}^{s,(2)}}{\tau^s} \right|^{n+1} \tag{35}$$

subject to full constraints equation (13)

$$\begin{aligned} 0 = \epsilon_j^{\mathrm{G}} &- w \sum_{s=1}^{S} \mathbf{m}_j^{s,(1)} \left| \frac{\boldsymbol{\sigma}^{(1)} : \mathbf{m}^{s,(1)}}{\tau^s} \right|^{n} \operatorname{sign}(\boldsymbol{\sigma}^{(1)} : \mathbf{m}^{s,(1)}) \\ &- (1-w) \sum_{s=1}^{S} \mathbf{m}_j^{s,(2)} \left| \frac{\boldsymbol{\sigma}^{(2)} : \mathbf{m}^{s,(2)}}{\tau^s} \right|^{n} \operatorname{sign}(\boldsymbol{\sigma}^{(2)} : \mathbf{m}^{s,(2)}) \end{aligned} \tag{36}$$

for $j = 1, \ldots, 5$ requires that

$$\boldsymbol{\sigma}^{(1)} = \boldsymbol{\sigma}^{(2)}. \tag{37}$$

If λ_j, $j = 1, \ldots, 5$, are Lagrange multipliers, and

$$\mathscr{L} = w\sum_{s=1}^{S}\tau_s\left|\frac{\boldsymbol{\sigma}^{(1)}:\mathbf{m}^{s,(1)}}{\tau^s}\right|^{n+1} + (1-w)\sum_{s=1}^{S}\tau_s\left|\frac{\boldsymbol{\sigma}^{(2)}:\mathbf{m}^{s,(2)}}{\tau^s}\right|^{n+1}$$
$$+\lambda_j\left[\epsilon_j^{\mathrm{G}} - w\sum_{s=1}^{S}\mathbf{m}_j^{s,(1)}\left|\frac{\boldsymbol{\sigma}^{(1)}:\mathbf{m}^{s,(1)}}{\tau^s}\right|^{n}\mathrm{sign}(\boldsymbol{\sigma}^{(1)}:\mathbf{m}^{s,(1)})\right.$$
$$\left.-(1-w)\sum_{s=1}^{S}\mathbf{m}_j^{s,(2)}\left|\frac{\boldsymbol{\sigma}^{(2)}:\mathbf{m}^{s,(2)}}{\tau^s}\right|^{n}\mathrm{sign}(\boldsymbol{\sigma}^{(2)}:\mathbf{m}^{s,(2)})\right], \tag{38}$$

where summation over the repeated index j is implied, then the constrained relative extrema of $\dot{W}_{\mathrm{i}}$ are given by

$$\frac{\partial\mathscr{L}}{\partial\sigma_j^{(1)}} = \frac{\partial\mathscr{L}}{\partial\sigma_j^{(2)}} = \frac{\partial\mathscr{L}}{\partial\lambda_j} = 0. \tag{39}$$

Equation (39) is satisfied if

$$\lambda_j = \frac{n+1}{n}\sigma_j^{(1)} = \frac{n+1}{n}\sigma_j^{(2)}, \quad j = 1,\ldots,5, \tag{40}$$

which implies equation (37).

To show that equation (37) characterizes not only a relative, but also the absolute (global) minimum, all we need show is that the stress–strain rate relation, equation (36), can be derived from a potential $F(\boldsymbol{\sigma}^{\mathrm{G}})$ according to

$$\dot{\boldsymbol{\varepsilon}}^{\mathrm{G}} = \frac{\partial F}{\partial\boldsymbol{\sigma}^{\mathrm{G}}}(\boldsymbol{\sigma}^{\mathrm{G}}), \tag{41}$$

where $F(\boldsymbol{\sigma}^{\mathrm{G}})$ is concave to the origin (Hill (1950, chap. 2)) in stress space

$$F(\boldsymbol{\sigma}^{\mathrm{G}}) = \frac{w}{n+1}\sum_{s=1}^{S}\tau_s\left|\frac{\boldsymbol{\sigma}^{\mathrm{G}}:\mathbf{m}^{s,(1)}}{\tau^s}\right|^{n+1} + \frac{1-w}{n+1}\sum_{s=1}^{S}\tau_s\left|\frac{\boldsymbol{\sigma}^{\mathrm{G}}:\mathbf{m}^{s,(2)}}{\tau^s}\right|^{n+1} \tag{42}$$

is such a potential.

Similar considerations apply also in the case that the FC constraints, equation (36), are replaced by RC constraints, equation (22), provided that $\sigma_3^{\mathrm{G}} = \sigma_5^{\mathrm{G}} = 0$.

APPENDIX B

Estimating $\dot{W}_b$ and $\dot{W}_c$

We consider first the power stored in DBBs, $\dot{W}_{\mathrm{b}}$. Given the dislocation density ρ, shear modulus G, Burgers vector magnitude b, and dislocation interaction parameter $0 \le \alpha \le 0.5$, the stored energy per unit volume, i.e. the stored energy density, is approximately (Hughes *et al.* 2003)

$$\alpha\rho G b^2. \tag{43}$$

Now, according to Kröner's formula (Ortiz *et al.* 2003), the dislocation density tensor $\mathbf{A}$ between two bands that have deformation gradients $\mathbf{F}^{(1)}$ and $\mathbf{F}^{(2)}$ is

$$\mathbf{A} = [\mathbf{F}] \times \mathbf{n}/\delta_{\mathrm{b}}, \tag{44}$$

where $[\mathbf{F}] = \mathbf{F}^{(2)} - \mathbf{F}^{(1)}$ denotes the jump in deformation gradient across an interface of thickness δ_{b} (see figure 2) with normal $\mathbf{n}$. Recalling that (Nye 1953)

$$\mathbf{A} = \sum_{s=1}^{S} \rho^s \boldsymbol{\beta}^s \otimes \boldsymbol{\xi}^s, \tag{45}$$

where ρ^s is the dislocation density with (non-unit) Burgers vector β^s, $\|\beta^s\| = b$, $\forall s$, and unit line direction vector $\boldsymbol{\xi}^s$. The norm of $\mathbf{A}$, $\|\mathbf{A}\| = \sqrt{\mathbf{A} : \mathbf{A}}$, is therefore of the order $\|\mathbf{A}\| \approx (\sum_s \rho^s)b = \rho b$. Then, the approximate energy stored per unit DBB volume in a grain whose bands have deformation gradients $\mathbf{F}^{(1)}$ and $\mathbf{F}^{(2)}$ is $\alpha G b \|\mathbf{A}\|$. Assuming the grain to be a sphere of diameter D, and assuming that N DBB form in the grain, the volume of DBB per unit grain volume goes as $ND^2\delta_\mathrm{b}/D^3$, so that the stored energy per unit grain volume is given by $\kappa_\mathrm{b} N \alpha G b \delta_\mathrm{b} \|\mathbf{A}\|/D$, where we have absorbed all the uncertainties of estimation into the parameter κ_b.

We are interested in the stored *power* density at the instant of banding. Thus,

$$\dot{W}_\mathrm{b} = \kappa_\mathrm{b} \left(\frac{N \alpha G b}{D} \right) \frac{\mathrm{d}\|[\mathbf{F}] \times \mathbf{n}\|}{\mathrm{d}t}, \tag{46}$$

which is independent of δ_b. Let $\mathbf{F}_0$ be the deformation gradient of the grain and $\mathbf{L}_0^{(1)}$ and $\mathbf{L}_0^{(2)}$ their respective velocity gradients at the instant of deformation banding. By definition, at the instant of banding, each band of the grain has the same deformation gradient, so that $[\mathbf{F}_0] = \mathbf{0}$ across any plane. Let $\mathbf{F}_t^{(1)}$ and $\mathbf{F}_t^{(2)}$ be the deformation gradient of the bands at time t after their formation. Then, to a good approximation, if t is small, according to equation (7), $\mathbf{F}_t^{(i)} = \mathbf{F}_0 + t\mathbf{L}_0^{(i)}\mathbf{F}_0$, for $i = 1, 2$. Thus, $[\mathbf{F}_t] = t[\mathbf{L}_0]\mathbf{F}_0$. Rewriting equation (46) as

$$\dot{W}_\mathrm{b} = \kappa_\mathrm{b} \frac{N \alpha G b}{D} \lim_{t \downarrow 0} \frac{\|[\mathbf{F}_t] \times \mathbf{n}\| - \|[\mathbf{F}_0] \times \mathbf{n}\|}{t}, \tag{47}$$

and applying the preceding conclusions, results in

$$\dot{W}_\mathrm{b} = \kappa_\mathrm{b} \frac{N \alpha G b}{D} \|[\mathbf{L}_0]\mathbf{F}_0 \times \mathbf{n}\|. \tag{48}$$

We next turn toward estimating $\dot{W}_\mathrm{c}$. As already noted, homogeneously deforming grains in a Taylor polycrystal are compatible across the grain boundary. The average deformation gradient of a grain, $\mathbf{F}^\mathrm{G}$, with two bands whose grain relative volume fractions are w and $1 - w$ and whose individual deformation gradients are $\mathbf{F}^{(1)}$ and $\mathbf{F}^{(2)}$, respectively, is

$$\mathbf{F}^\mathrm{G} = w\mathbf{F}^{(1)} + (1 - w)\mathbf{F}^{(2)}. \tag{49}$$

By deforming inhomogeneously, the grain creates incompatibilities at the grain boundary, as shown in figure 2, which are to be accommodated through inhomogeneous deformations at the grain boundary through the generation and storage of GND.

To approximate $\dot{W}_\mathrm{c}$ in equation (1), we use an argument similar to that of Ashby (1970). Consider the difference in deformation (physically, a void or material interpenetration) that will be created in a band of length equal to the grain diameter D due to its deformation with gradient $\mathbf{F}^{(1)}$ instead of $\mathbf{F}^\mathrm{G}$. We may regard $\|\mathbf{F}^{(1)} - \mathbf{F}^\mathrm{G}\|D$ as a scalar measure of this deformation difference. To fill this difference will take $\|\mathbf{F}^{(1)} - \mathbf{F}^\mathrm{G}\|D/b$ GND, where b is the magnitude of the GND Burgers vector. If there are $N + 1$ DBs in the grain, half $((N + 1)/2)$ of which have volume fraction w, and the other half have volume fraction $1 - w$, the grain boundary area corresponding to the first type of band goes as $2D^2 w/(N + 1)$. So, the dislocation density ρ needed to

accommodate the first type of band goes as $(N+1)\|\mathbf{F}^{(1)}-\mathbf{F}^{G}\|/(2Dbw)$, and according to equation (43), the stored energy goes as $\alpha Gb(N+1)\|\mathbf{F}^{(1)}-\mathbf{F}^{G}\|/(2Dw)$. As shown in figure 2, let δ_c be the thickness of the accommodation layer at the grain boundary, where the GND form by inhomogeneous deformation. Then, the volume fraction of the accommodation layer in the first type of bands is $D^2\delta_c w/D^3 = w\delta_c/D$, so that the stored energy density in the first type of bands (with deformation gradient $\mathbf{F}^{(1)}$) is $(\alpha Gb\delta_c(N+1)/(2D^2))\|\mathbf{F}^{(1)}-\mathbf{F}^{G}\|$, which is independent of w. Similarly, the stored energy density in the second type of bands (with deformation gradient $\mathbf{F}^{(2)}$) is $(\alpha Gb\delta_c(N+1)/(2D^2))\|\mathbf{F}^{(2)}-\mathbf{F}^{G}\|$.

Observing from equation (49) that $\mathbf{F}^{(1)}-\mathbf{F}^{G}=(1-w)[\mathbf{F}]$, and $\mathbf{F}^{(2)}-\mathbf{F}^{G}=w[\mathbf{F}]$, and summing the two stored energy contributions above, we have

$$W_c = \frac{\alpha Gb(N+1)\delta_c}{2D^2}\|[\mathbf{F}]\|. \tag{50}$$

Thus,

$$\dot{W}_c = \frac{\alpha Gb(N+1)\delta_c}{2D^2}\lim_{t\downarrow 0}\frac{\|[\mathbf{F}_t]\|-\|[\mathbf{F}_0]\|}{t}. \tag{51}$$

Using arguments similar to those preceding equation (48), and letting $N+1\approx N$, in view of the considerable assumptions made, we finally have

$$\dot{W}_c = \frac{N}{2}\frac{\alpha Gb\delta_c}{D^2}\|[\mathbf{L}_0]\mathbf{F}_0\|. \tag{52}$$

References

Ahlborn, H., 1966a, *Recrystallization, Grain Growth, and Textures* (Metals Park, OH: ASM), p. 374; 1966b, *Z. Metallk.*, **57**, 877.

Akef, A., and Driver, J. H., 1991, *Mater. Sci. Engng* A, **132**, 245.

Argon, A. S., 2002, *Scripta mater.*, **47**, 683.

Asaro, R. J., and Needleman, A., 1985, *Acta metall.*, **33**, 923.

Ashby, M. F., 1970, *Phil. Mag.*, **21**, 399.

Barrett, C. S., 1939, *Trans. AIME*, **135**, 296.

Barrett, C. S., and Levenson, L. H., 1940, *Trans. AIME*, **137**, 112.

Basson, F., and Driver, J. H., 2000, *Acta mater.*, **48**, 2101.

Bay, B., Hansen, N., Hughes, D. A., and Kuhlmann-Wilsdorf, D., 1992, *Acta metall. mater.*, **40**, 205.

Bishop, J. F. W., and Hill, R., 1951a, *Phil. Mag.*, **42**, 1298; 1951b, *Phil. Mag.*, **42**, 414.

Canova, G. R., Fressengeas, C., Molinari, A., and Kocks, U. F., 1988, *Acta metall.*, **38**, 1961.

Chin, G. Y., and Mammel, W. L., 1969, *Trans. AIME*, **245**, 1211.

Chin, G. Y., and Wonsiewicz, B. C., 1969, *Trans. AIME*, **245**, 871.

Christoffersen, H., and Leffers, T., 1998, *Acta mater.*, **46**, 4093.

Cizek, P., Parker, B. A., and Wynne, B. J., 1995, *Scripta metall.*, **32**, 319.

Dawson, P. R., Mika, D. P., and Barton, N. R., 2002, *Scripta mater.*, **47**, 713.

Dillamore, I. L., and Katoh, H., 1974 , *Metal Sci.*, **8**, 21.

Duggan, B. J., and Lee, C. S., 1996, Proceedings of the Eleventh International Conference on Textured Materials (ICOTOM 11), edited by Z. Liang, L. Zuo and Y. Chu (Xian, China: International Academic Publishers).

Duggan, B. J., Liu, G. L., and Zhang, L. X., 1998, *Mater. Sci. Forum*, **273–275**, 291.

Gurtin, M. E., 1981, *An Introduction to Continuum Mechanics* (New York: Academic Press).

Hansen, N., and Jensen, D. J., 1999, *Phil. Trans. R. Soc. Lond.* A, **357**, 1447.

Hill, R., 1950, *The Mathematical Theory of Plasticity* (Oxford: Clarendon Press); 1961, *Progress in Solid Mechanics*, vol. 2, edited by I. N. Sneddon and R. Hill (New York: Interscience), chap. 6; 1967, *J. Mech. Phys. Solids*, **15**, 79.

HOSFORD, W. F., 1993, *The Mechanics of Crystals and Textured Polycrystals* (New York: Oxford University Press).
HUANG, X., 1998, *Scripta mater.*, **38**, 1697.
HUANG, X., and HANSEN, N., 1997, *Scripta mater.*, **37**, 1.
HUGHES, D. A., and HANSEN, N., 1993, *Met. Trans.*, **24A**, 2021; 1997, *Acta mater.*, **45**, 3871.
HUGHES, D. A., HANSEN, N., and BAMMANN, D. J., 2003, *Scripta mater.*, **48**, 147.
HUGHES, D. A., LIU, Q., CHRZAN, D. C., and HANSEN, N., 1997, *Acta mater.*, **45**, 105.
HUMPHREYS, F. J., and ARDAKANI, M. G., 1994, *Acta metall. mater.*, **42**, 749.
HUTCHINSON, J. W., 1976, *Proc. R. Soc. Lond.* A, **348**, 101.
KOCKS, U. F., TOMÉ, C. N., and WENK, H. R., 1998, *Texture and Anisotropy* (Cambridge: Cambridge University Press).
KUHLMANN-WILSDORF, D., 1999a, *Acta mater.*, **47**, 1697; 1999b, *Phil. Mag.* A, **79**, 955.
KULKARNI, S. S., JR, and KUHLMANN-WILSDORF, D., 1998, *Acta mater.*, **46**, 5283.
LEBENSOHN, R. E., and TOMÉ, C. N., 1993, *Acta metall. mater*, **41**, 2611.
LEE, C. S., and DUGGAN, B. J., 1991, *Met. Trans.* A, **22A**, 2637; 1993, *Acta metall. mater.*, **41**, 2691.
LEE, C. S., DUGGAN, B. J., and SMALLMAN, R. E., 1993, *Acta metall. mater.*, **41**, 2265.
LEE, C. S., SMALLMAN, R. E., and DUGGAN, B. J., 1995, *Scripta metall. mater.*, **33**, 727.
LI, Z. J., GODFREY, A., and LIU, Q., 2004, *Acta mater.*, **52**, 149.
LIU, G., and DUGGAN, B. J., 2001, *Metall. Mater. Trans.* A, **32A**, 125.
LIU, Q., and HANSEN, N., 1998, *Proc. R. Soc. Lond.* A, **454**, 2555.
LIU, Q., HUANG, X., LLOYD, D. J., and HANSEN, N., 2002, *Acta mater.*, **50**, 3789.
LIU, Q., WERT, J., and HANSEN, N., 2000, *Acta mater.*, **48**, 4267.
MAHESH, S., Tomé, C. N., MCCABE, R. J., KASCHNER, G., BEYERLEIN, I. J., and MISRA, A., 2004, *Metall. mater. Trans.* (accepted).
MAURICE, C., and DRIVER, J. H., 1993 , *Acta metall. mater.*, **41**, 1653.
MEYERS, M. A., and ASHWORTH, E., 1982 , *Phil. Mag.* A, **46**, 737.
NYE, J. F., 1953, *Acta metall.*, **1**, 153.
ORTIZ, M., and REPETTO, E. A., 1999, *J. Mech. Phys Solids*, **47**, 397.
ORTIZ, M., REPETTO, E. A., and STAINIER, L., 2000, *J. Mech. Phys. Solids*, **48**, 2077.
PEETERS, B., SEEFELDT, M., TEODOSIU, C., KALIDINDI, S. R., HOUTTE, P. V., and AERNOUDT, E., 2001, *Acta mater.*, **49**, 1607.
READ, W. T., and SHOCKLEY, W., 1950, *Phys. Rev.*, **78**, 275.
SIL, D., and VARMA, S. K., 1993, *Met. Trans.* A, **24A**, 1153.
SPELLUCCI, P., 1998, *Math. Prog.*, **82**, 413. FORTRAN code donlp2: do nonlinear programming, obtainable via anonymous ftp from netlib.org as netlib/opt/donlp2.
TJERKSTRA, H. H., 1961, *Acta metall.*, **9**, 259.
TOMÉ, C., CANOVA, G. R., KOCKS, U. F., CHRISTODOULOU, N., and JONAS, J. J., 1984, *Acta metall.*, **32**, 1637.
TSE, Y. Y., LIU, G. L., and DUGGAN, B. J., 2000, *Scripta mater.*, **42**, 25.
WERT, J. A., 2002, *Acta mater.*, **50**, 3125.
WERT, J. A., and HUANG, X., 2003, *Phil. Mag.*, **83**, 969.
WINTHER, G., 2003, *Acta mater.*, **51**, 417.
WINTHER, G., HUANG, X., and HANSEN, N., 2000, *Acta mater.*, **48**, 2187.
WINTHER, G., JENSEN, D. J., and HANSEN, N., 1997, *Acta mater.*, **45**, 5059.